RICE UNIVERSITY

The Application of Finite Element Methods to Aeroelastic Lifting Surface Flutter

by

Matthew Lucas Guertin, 2d Lt USAF

A THESIS SUBMITTED
IN PARTIAL FULFILLMENT OF THE
REQUIREMENTS FOR THE DEGREE

Master of Science

APPROVED, THESIS COMMITTEE

Dr. John E. Akin, Chair
Professor of Mechanical Engineering and Materials Science

Dr. Andrew J. Meade
Professor of Mechanical Engineering and Materials Science

Dr. Ilinca Stanciulescu
Assistant Professor of Civil Engineering

HOUSTON, TEXAS
April 2012

ABSTRACT

The Application of Finite Element Methods to Aeroelastic Lifting Surface Flutter

by

Matthew Lucas Guertin, 2d Lt USAF

Aeroelastic behavior prediction is often confined to analytical or highly computational methods, so I developed a low degree of freedom computational method using structural finite elements and unsteady loading to cover a gap in the literature. Finite elements are readily suitable for determination of the free vibration characteristics of eccentric, elastic structures, and the free vibration characteristics fundamentally determine the aeroelastic behavior. I used Theodorsen's unsteady strip loading formulation to model the aerodynamic loading on linear elastic structures assuming harmonic motion. I applied Hassig's 'p-k' method to predict the flutter boundary of nonsymmetric, aeroelastic systems. I investigated the application of a quintic interpolation assumed displacement shape to accurately predict higher order characteristic effects compared to linear analytical results. I show that quintic interpolation is especially accurate over cubic interpolation when multi-modal interactions are considered in low degree of freedom flutter behavior for high aspect ratio HALE aircraft wings.

Acknowledgments

I would like to thank my advisor, Dr. Akin, for his patience and willingness to help and guide me through the learning process of this project. I'm honored to study under such a knowledgeable and understanding advisor and I'm obliged to have the academic freedom to study a topic of significant personal and professional interest. I would also like to thank Dr. Meade and Dr. Stanciulescu for their help and advice as members of my thesis committee.

I would also like to thank my fellow graduate students Thomas "Woody" Sukut and Anthony Puntel as well as all the other Rice University Air Force members for their support and motivation. Woody thanks for being my study buddy. Tony thanks for not being so serious. Good luck in your Air Force careers. I would also like to thank my family for their love, support and prayers, which have sustained me.

Disclaimer

The views expressed in this article are those of the author and do not reflect the official policy or position of the United States Air Force, Department of Defense, or the U.S.

Contents

List of Figures

List of Tables

Nomenclature

A	structural inertia matrix
AA	aerodynamic axis (line)
AC	aerodynamic center (point)
AR	aspect ratio
b	semi-chord
B	aerodynamic damping matrix
$\boldsymbol{B}^*$	binary aerodynamic damping matrix
c	chord length
C	aerodynamic stiffness matrix
$\boldsymbol{C}^*$	binary aerodynamic stiffness matrix
CFD	Computational Fluid Dynamics
CG	center of mass (point)
CP	control point (point)
D	structural damping matrix
DOF	degree of freedom
E	structural stiffness matrix
EI	beam bending rigidity
FA	flexural axis (line)
FD	frequency domain
FE	finite element
GJ	beam torsional rigidity
HALE	High-Altitude Long Endurance
ISA	International Standard Atmosphere
L	lift force
LCO	limit cycle oscillations
LE	leading edge
k	reduced frequency ($k = \omega b/V$)
M	moment due to lift force about SC
MDOF	multiple degrees of freedom
MA	mass axis (line)
SC	shear center (point)
SDOF	single degree of freedom
TD	time domain
w	bending displacement (+ up)
α	pitch displacement (+ LE up)
$\varphi, \dot{\varphi}, \ddot{\varphi}$	generalized coordinate, rate, acceleration
λ, ϕ	real eigenvalue, eigenvector
$\tilde{\lambda}, \tilde{\phi}$	complex eigenvalue, eigenvector
θ	torsional displacement
ω	modal (natural) frequency
ζ	damping ratio

Chapter 1

Introduction

"Adde parvum parvo magnus acervus erir"

"Add little to a little and there will be a great heap"

~Ovid, Latin poet [1].

1.1. Aeroelasticity Defined

Aeroelasticity is the field of study concerned with the interaction between the deformation of an elastic structure in an airstream and the resulting coupled effect on the aerodynamics and structural dynamics [2]. The interdisciplinary convolution of the components of aeroelasticity is best illustrated by a Venn diagram or Collar triangle in Figure 1.1, which shows how the ternary component forces interact to produce aeroelastic phenomenon such as flutter [2–7].

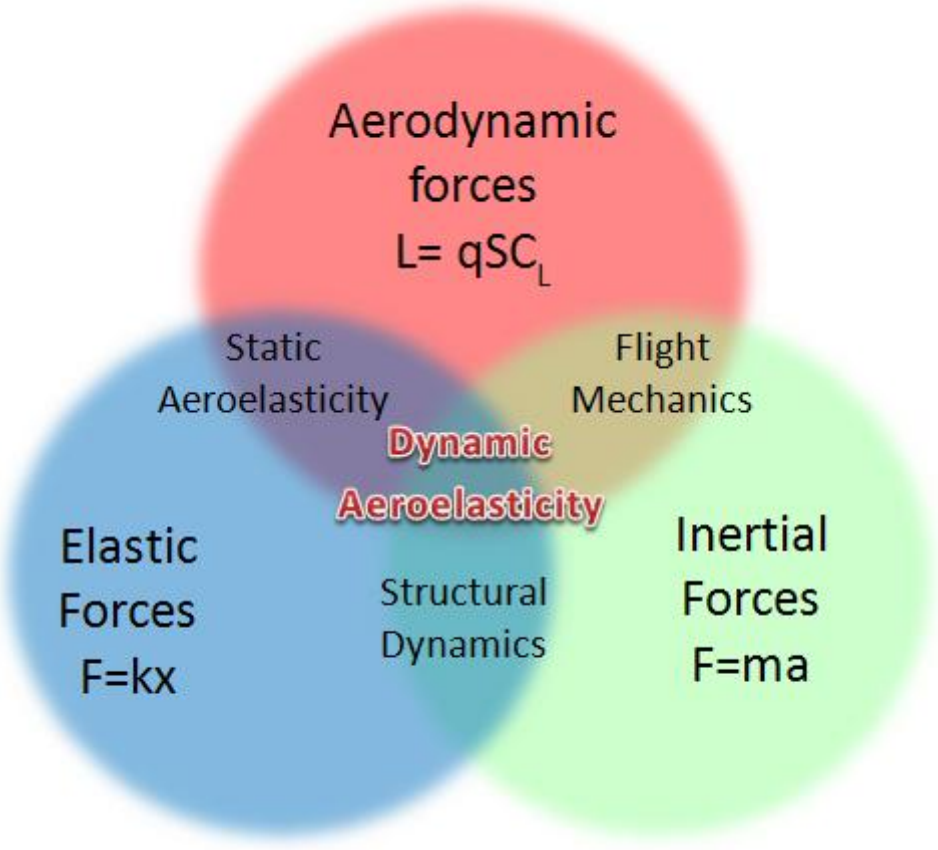

Figure 1.1 – Collar aeroelastic Venn diagram

1.2. Motivation

A study of aeroelastic phenomena in wings structures is of great importance to the continued development and design of advanced aircraft as radical designs are utilized to capture maximum performance. Determination of the aeroelastic behavior of a simplified wing-like structure is a fundamental aspect of industrial practice in flight vehicle design, and is a historical starting point for complex airframe analysis [5]. The *finite element method* (FEM) is well suited for the determination of structural vibrational characteristics. Coupling the FEM with accurate lifting load prediction techniques such as strip theory or the vortex panel

method serves as a pre-design, and airworthiness check tool [5] for many aircraft design industries. Thus, a detailed understanding of the FEM, lifting load techniques, and an integration of both disciplines is important for new aerospace engineers.

The original purpose of this thesis was to produce a teaching tool for the application of the FEM and simplified lifting load prediction to aeroelastic analysis. Basic knowledge of flight mechanics is assumed since such a discussion is a related but independent field. This project will focus primarily on fixed wing lifting surface structural dynamic response, in particular flutter. The contributions herein are derived from modern courses and texts in aeroelasticity in order to further an understanding of the related material necessary for aeroelastic analysis, and to explore the "black box" elements of many commercial techniques.

1.3. Thesis Overview

Chapters 2, 3, and 4 constitute background material on structural dynamics, the FEM and steady aerodynamics necessary for an understanding of dynamic aeroelastic flutter. Chapter 2 covers the history and importance of aeroelastic analysis. Chapter 3 addresses the structural dynamics fundamental to dynamic aeroelasticity, specifically coupled bending and torsional vibrations of wing like structures. Chapter 4 presents a simplified aeroelastic model to demonstrate the coupling of structural and aero forces independent of structural inertia.

Chapters 5 and 6 incorporate unsteady aerodynamics coupled with a structural FEM model for the prediction of critical aeroelastic flutter behavior.

Chapter 5 introduces the phenomenon of dynamic flutter as a time varying response to harmonic loading, with the inclusion of structural inertia. Chapter 6 presents a description of the computational lifting strip method joined with a structural FEM model for the prediction of aeroelastic behavior.

Chapter 2

Literature of Aeroelastic Analysis

As mentioned in the introduction, aeroelasticity is a ternary interaction of inertial, elastic and fluid forces on a structure. The study of aeroelasticity requires prior study of all constituent fields in regard to each applied component of the problem: dynamics, solid mechanics, and aerodynamics, respectively [4]. The coupling of any two of these fields produces an outgrowth in its own right, such as the coupling of dynamics and solid mechanics to produce structural dynamics (vibration), or the coupling of aerodynamics and solid mechanics to produce static aeroelasticity. These two dual coupled fields will be addressed in this thesis prior to the full ternary coupling phenomenon of dynamic aeroelasticity.

There are, of course, many other forces that can influence aeroelastic characteristics in a range of flight conditions such as thermal radiation, chemical disassociation, and shock wave interaction [8] that fall under the study of *aerothermoelasticity*, but such a discussion is beyond the scope of this report. Aeroelastic phenomenon is also typically and historically observed in flight control systems termed *aeroservoelasticity* [4], but this study will focus on the derivation

and description of lifting surface flutter. The same principles apply to aeroservoelasticity, but require a study of control methods [9].

2.1. Historical Aeroelastic Analysis

The study of flutter and aeroelasticity in general is of utmost importance to the aerospace industry as a design driver even in the early days of flight. The first success of the Wright Flyer in late 1903 is due in large part to a consideration of aeroelastic effects. The Wright brothers developed a "wing warping" mechanism for lateral control [3], which allowed for controllability without drastically altering the local wing camber [10]. The brothers also recognized an adverse aeroelastic effect on the efficiency of the propeller blades and corrected it with backward sweep, which maintained the total lift while moving the spanwise center of pressure inboard [10]. However, just days prior to the Wright brother's success, Samuel Langley unsuccessfully attempted powered flight in his monoplane, which crashed into in the Potomac due to a lack of torsional rigidity [7] as shown in Figure 2.1. Excessive wing twist caused by high wing camber coupled with low torsional stiffness resulted in wing structural failure. Similar aeroelastic phenomenon in other monoplane designs resulted in the dominance of biplane designs for 30 years until the advent of semi-monocoque structures [3].

The first recorded and documented occurrence of aircraft flutter was the Handley Page O/400 bomber in 1916 by F. W. Lanchester as shown in Figure 2.1. The plane experienced violent in-flight asymmetric torsional oscillation of the

fuselage and pitch oscillation of elevators due to a lack of torsional stiffness between the independent port and starboard elevators [3, 5, 7]. Lanchester discovered that the oscillations were not due to any resonance of vibration sources, such as the engine, but were self-excited by an interaction with airflow [7].

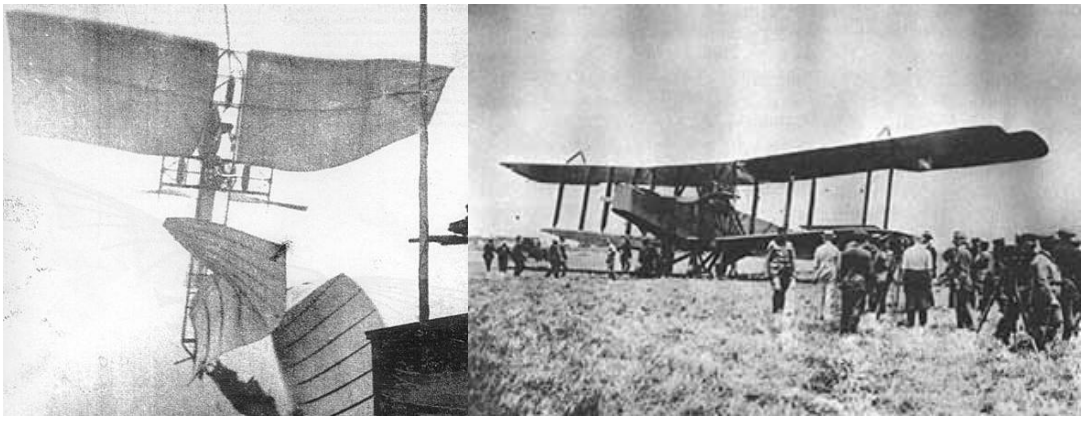

Figure 2.1 – Langley Flyer and Hanley-Page O/400 bomber [11]

These two historical failure cases are indicative of the two major aeroelastic failure modes: *static aeroelasticity* and *dynamic aeroelasticity* [6]. The former mode considers the nonoscillatory interaction of aerodynamics and solid mechanics where inertial forces do not play a significant role. The case of the Langley flyer failure points to a case of static *divergence* of the wing structure once the aerodynamic forces caused the wing to twist beyond the structural restoring moment capacity. The primary design considerations to prevent static failure are structural stiffness, and load redistribution due to a change in the effective wing chamber.

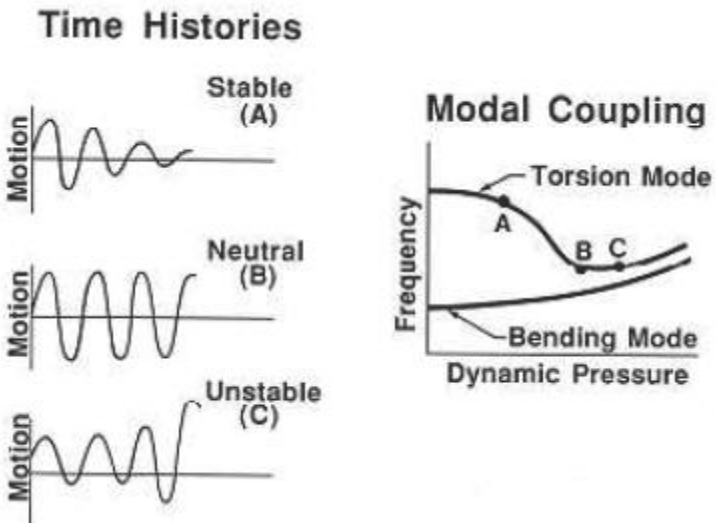

Figure 2.2 – Modal coupling as a result of convolution and corresponding disturbance time history [10]

Dynamic aeroelasticity or *flutter* incorporates the oscillatory effects of the ternary interaction previously discussed. Classic flutter is a non-conservative mechanics problem and is an extension of the static cases. Since all non-conservative loading problems contain dynamic effects, classic flutter is a more accurate representation of aeroelasticity. The case of the Handley Page O/400 bomber is an example of a combination of two or more modes of vibration coalescing to extract energy from the airstream to create flutter as shown in Figure 2.2. The frequencies at point A are well separated and the motion damps out over time. At point B, any initial disturbance, such as a wind gust, will produce harmonic limit cycle oscillations (LCO), which can lead to fatigue failure. Any operation at point C can result in immediate failure as the disturbance grows bounded by nonlinear effects [10]. It is important to note that flutter is not a forced resonant response as discovered by Lanchester, since the airflow is initially steady prior to an interaction with the system. The destruction of the Tacoma Narrows Bridge in 1940

is often falsely attributed to resonance [12], when in fact, the failure was due to a form of torsional self-excitation caused by vortex shedding

2.2. Aeroelastic Modeling

The hallmark of a good model is simplicity in design and ease of interpretation. There are many considerations in the ternary interactions of aeroelasticity in full aircraft structures, but a simplified model can provide realistic physical predictions with appropriate parameters. In a review of the state-of-the-art in 1970, Dowell [13] categorizes all panel flutter research and models into four types. Neglecting nonlinear aerodynamic modeling, such as computational fluid dynamics (CFD) methods, the model types still apply today to general aeroelastic analysis and are outlined in Table 2.1.

Table 2.1 – Types of flutter analysis

Model Types	Quasi-steady aerodynamics	Linearized aerodynamics	CFD
Linear Structural	**Type 1**	**Type 2**	***Type 5**
Nonlinear Structural	**Type 3**	**Type 4**	***Type 6**

Dowell's categories are based on the structural and aerodynamic theories employed: 1) Linear structural theory; quasi-steady aerodynamic theory [14]; 2)

linear structural theory; full linearized (inviscid, potential, finite-state) aerodynamic theory [15]; 3) nonlinear structural theory; quasi-steady aerodynamics [16]; 4) nonlinear structural theory; full linearized aerodynamic theory [17]. Type 4) is the most general, and type 1) is the simplest but has two major drawbacks: a) structural nonlinearities are not considered, thus only the flutter boundary can be predicted accurately with no information regarding the actual flutter oscillations; b) the use of quasi-steady aerodynamics neglects unsteadiness and three-dimensional effects and cannot be used in the transonic region where flutter is most likely to occur.

One could include an additional 2 types of flutter analysis shown as Type 5 and Type 6. Those analyses include coupled nonlinear CFD, fluid-structure interaction, aerodynamic models with some consideration for turbulence, and other three-dimensional effects. However, the combination of aerodynamic and structural nonlinearities adds enormous complexity to the flutter analysis problem, and often does not influence the flutter boundary characteristics [15, 18]. Additionally, many three-dimensional effects, such as boundary layer interaction or wingtip downwash, minimally affect the behavior of long slender wings in subsonic cruise.

Regardless of the structural/inertial or aerodynamic model employed, there are certain basic mathematical requirements to accurately capture aeroelastic behavior. The model must represent the vibration behavior over a range of interest, usually 0-40 Hz for streamlined commercial jet liners and 0-60 Hz for streamlined military aircraft [5]. The vibration characteristics of large bluff body stationary structures such as a cable stayed bridges are typically one or two orders of

magnitude lower at 0.1-1 Hz [19]. However, the flutter characteristics of bluff and streamlined bodies differ substantially based on the *Kutta condition*, which requires smooth, attached flow at the sharp trailing edge of streamlined bodies [20]. The model must also yield mode shapes, natural frequencies and modal masses in the range of interest [5].

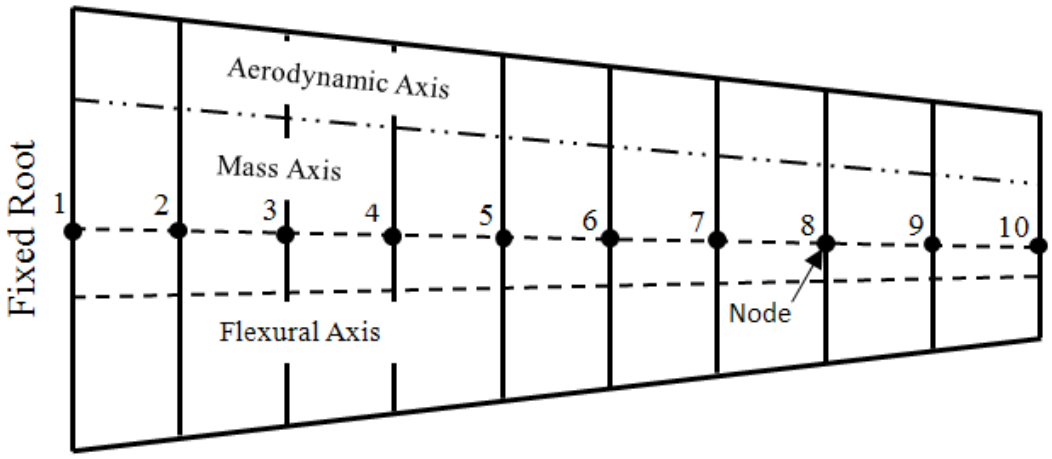

Figure 2.3 – Low DOF cantilever wing model

The complexity of the model is necessity dependent and this thesis will focus on a pre-design phase style, low DOF model commensurate with a teaching tool objective. Many low DOF analyses include only *binary* or two DOF behaviors (bending and torsion), which are typically investigated analytically. The common alternatives are highly computational CFD-FEM methods. However, one can show that a low DOF model, as shown in Figure 2.3, with proper simplifying assumptions can accurately predict flutter behavior.

2.2.1. Structural/Inertial Model

The prediction of flutter behavior is conveniently and classically formulated in matrix terms. In fact, the origin and development of Matrix Structural Analysis (MSA), a precursor to the FEM, naturally lies in the field of aeroelasticity [21]. The nomenclature familiar in the application of FEM originates from a MSA source book coauthored by Collar [22], the developer of the aeroelastic triangle. The genesis of the structural element can also be traced to the work of Duncan and Collar[23] who pioneered the application to the numerical analysis of propeller blades [2]. The modern FEM application is the use of *beam elements* to model wings and aircraft components. The modified beam element is capable of bending, twisting, shear and axial deformation. Thus, when a wing is broken into small components, the vibration characteristics can be accurately modeled with a small number of elements placed along a reference axis [5]. The mass of the structure is then distributed along the nodes of the individual beam elements.

The structural model employed in this study is linear, in that it is a model for which the principle of superposition holds. Thus, the classical formulation of the modified bending and torsion beam element applies. The linear model is sufficient for flutter boundary determination, but does not accurately predict LCO behavior post flutter. However, even a linear structural model must consider coupled bending and torsion effects as a result of an offset between the sectional center of gravity and center of rotation. The vibrations of beams having noncollinear elastic and mass axes is a classical field of study with many sources [24–28], and is a foundation of general aeroelastic analysis.

2.2.2. Aerodynamic Model

The aerodynamic models used in this study for aeroelastic prediction are categorized as fully linearized in accordance with Dowell's type 2 and 4 aerodynamics. In this case, fully linearized means that the aerodynamic forces are represented as functions of non-dimensional coefficients with respect to a reference flight condition such as small variation in angle of attack and attached flow. Linearization has been extremely important in the development of aeroelastic analysis since the early days of simulation when nonlinear equations were practically impossible to solve computationally [29]. Linearized aerodynamic theories were pioneered by Theodorsen [30] and Collar [22], and serve as a foundation of aeroelastic analysis. Modern computational methods employ the general set of nonlinear equations, but linearized models can be used in all flight regimes with empirical correction.

2.2.2.1. Lifting surface flutter

The classical theories of aeroelasticity deal with the stability of an elastic structure in the wind. In typical elastic problems, the external forcing is prescribed and the stress and deformation can be considered independent of the forcing. When light aerodynamic structures are considered, the forcing inherently depends on the displacement of the structure, so typically there exists a critical wind speed where the aerodynamic forcing overcomes the elastic stiffness [20]. The classical approach to formulate the stability problem is to set up a system of homogeneous equations satisfied by a trivial solution or neutral stability in the case of flutter [4]. Since only the modes of deformation are of interest in a stability problem, it is acceptable to

consider the displacement as infinitesimal about equilibrium and the linearity of the flutter problem is uniquely justified. The classical formulation of the lifting surface flutter stability problem relies on the linearity assumption.

Theodorsen developed the classical unsteady lifting load strip model for harmonic motion, which directly applies to the stability characteristics of fluttering lifting surfaces [30, 31]. Theodorsen applies a frequency domain complex eigenvalue analysis to quantify the interaction of two or more vibrating modes in coalescence as observed by Lanchester [32]. The Theodorsen analysis applies to many classical stability boundary calculation techniques, most notably the determinate iteration method developed by Hassig [33]. Other stability analyses like swept wing divergence [34, 35], or composite geometry effects [36, 37] are covered extensively in the literature.

There are a number of textbooks that offer a complete analytical coverage of aeroelastic analysis including Fung [20], Bisplinghoff [6, 8], Hodges [3], Dowell [4], and Wright [5]. Many of the texts present a highly analytical formulation of the flutter problem with binary considerations, and only Hodges and Wright present an application of FE analysis for wing structures. The application of FE analysis to low order DOF systems is minimal in the literature [38] since stability characteristics are typically treated analytically. An assumed displacement shape of the Rayleigh-Ritz type is typical of analytical flutter approximations [39]. The application of FE analysis is more common in full scale industrial models where an entire aircraft structure is considered [15, 40].

2.2.2.2. Panel flutter

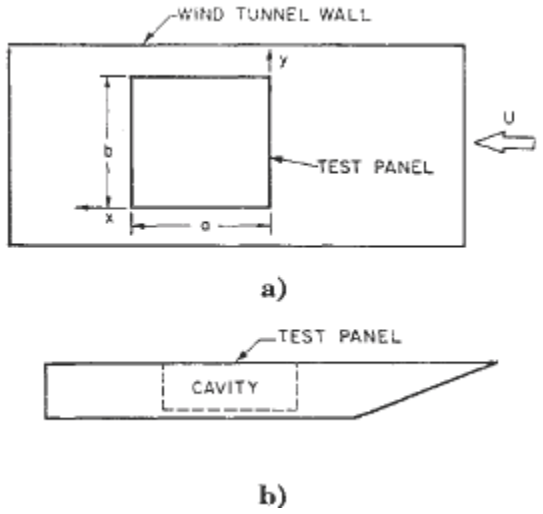

Figure 2.4 – Wall mounted surface panel [13]

Panel flutter is worth mentioning in an analysis of lifting surface flutter since the methods and research are similar and complementary. Panel flutter differs from lifting surface flutter since it is solely a supersonic phenomenon and only one side of the "panel" or plate is exposed to free stream flow while the other side is internal to the structure and experiences dead air [41]. The example diagram in Figure 2.4 illustrates a typical panel setup [13]

Panel flutter analysis and experimentation also employs simply supported and fixed-fixed boundary conditions since the panel represents the skin of the lifting surface, unlike lifting surface flutter which represents the entire wing structure. Panel flutter usually occurs as LCO at supersonic or hypersonic Mach for small plate like panels, but long fuselage like panels tend to experience extremely low frequency oscillations unlike any type of lifting surface flutter [13].

The use of FE analysis is well established for panel flutter prediction [14, 16, 41, 42], and one can apply the same principles to lifting surface flutter prediction. Olson (1967) extends beam a vibration problem to two-dimensional panel flutter considering only the two lower modes of plunge and plunge rate. Olson provides an explicit dynamic stiffness matrix with skew symmetric off diagonal terms consistent with a non-self-adjoint problem. The dynamic stiffness matrix presented is simply the addition of the symmetrical structural stiffness and asymmetric aerodynamic stiffness matrices. Weisshaar (1976) outlines a least-weight optimization study using finite elements and Type 1 panel flutter analysis. Mei (1977) extends the Olson paper to an FEM application of structural nonlinearities due to large amplitude oscillation. Grey (1991) further extends Mei's nonlinear method to hypersonic aerodynamics as is characteristic of many modern applications of panel flutter research [43, 44].

Chapter 3

Structural Vibration

Aeroelastic flutter is a classical and continuing problem in aeroelastic design and a full understanding begins with an analysis of the vibration characteristics of wing like structures. Flutter is characterized as an undesirable forced vibration type problem that can cause adverse structural dynamic effects. In general, the response of a system to external loads is dependent on the *natural frequencies* and the *damping* of the free system. While flutter behavior is not solely due to the application of external loads, but rather is due to self-excitation, the principles of forced vibration hold. As a subset of general forced vibration principles, harmonic motion will be assumed and investigated herein in the form given by

$$\varphi = \varphi_0 e^{\tilde{\lambda} t} \qquad 3.1$$

where φ is a generalized coordinate, φ_0 is the amplitude and $\tilde{\lambda}$ is the complex characteristic exponent describing the decay.

3.1. Equations of Motion

The equations of motion can be derived in a number of ways, but an energy method using Lagrange's equations offers a convenient formulation for any number of discrete generalized or physical coordinates. The formulation of the differential equation of motion for a dynamic system is given as [5]

$$\frac{d}{dt}\left(\frac{\partial T}{\partial \dot{\varphi}_i}\right) - \frac{\partial T}{\partial \varphi_i} + \frac{\partial \Im}{\partial \dot{\varphi}_i} + \frac{\partial U}{\partial \varphi_i} = \frac{\partial(\delta W)}{\partial(\delta \varphi_i)} = Q_{\varphi_i} \qquad 3.2$$

where T, U, and $\Im$ are the kinetic energy, potential energy and dissipative function, respectively. The kinetic energy term is given by the formulation

$$T = \frac{1}{2}\sum_i^n \sum_j^n A_{ij}\dot{\varphi}_i\dot{\varphi}_j, \qquad 3.3$$

the potential energy term considering only structural strain energy is given by

$$U = \frac{1}{2}\sum_i^n \sum_j^n E_{ij}\varphi_i\,\varphi_j, \qquad 3.4$$

and the dissipative function is given as an internal structural function of the generalized coordinate rate by

$$\Im = \frac{1}{2}\sum_i^n \sum_j^n D_{ij}\dot{\varphi}_i\dot{\varphi}_j. \qquad 3.5$$

The coefficients A_{ij}, E_{ij} and D_{ij} represent the structural inertia, stiffness, and damping, and $\varphi_{i\ldots j}$ is the ith or jth generalized coordinate of interest out of n DOF. The use of the terms *A, E, D* is to maintain consistency with later matrix formulation. The coefficients may be dependent on the generalized coordinates, but they are constant when only small displacements are considered, consistent with a linear structural system [8]. In the SDOF case, the coefficients are also scalar since $n = 1$.

On the right hand side of equation 3.2, Q_{φ_i} is the generalized force and δW is the virtual work done on the system, which in general has non-conservative components and conservative components not accounted on the left hand side of the equation [3]. The formulation for the non-conservative virtual work includes the external forcing minus the internal dissipation force

$$\delta W_{nc} = \delta W_o - \delta W_d = \left(f - \frac{\partial \Im}{\partial \dot{\varphi}}\right)\delta\varphi. \tag{3.6}$$

The internal dissipation is obviously represented in equation 3.2 on the left hand side of the equation in a form of structural damping. The formulation for the external virtual work ($f\delta q$) shown below includes point forces, spanwise (strip) forces and surface forces

$$\delta W_o = f_{point} \cdot \delta\varphi_i + \int_{span} f_{span} \cdot \delta\varphi_i dy \iint_{surf} f_{surf} \cdot \delta\varphi_i dxdy. \tag{3.7}$$

3.2. Free Vibration of Single Degree of Freedom Systems

The single degree of freedom (SDOF) system illustrates the concepts common to all dynamic systems, such as the inclusion of damping, and provides a starting point for general vibration analysis [45]. A discrete SDOF system is characterized by one rigid component with a flexible connection described by a single coordinate such as bending displacement or rotation. All SDOF systems are described by the same governing equation of motion with different symbols depending on the dynamics of interest. Continuous systems with flexible

components can be modeled as discrete systems as will be covered in the following sections, but the governing principles are the same.

The energy formulation can be applied to a cantilever wing to reduce the wing structure to a SDOF system with a tip mass for the purpose of an illustration of the principles of dynamic systems [45] as shown in Figure 3.1. If no external forcing is present in the SDOF system model, an application of equation 3.2 gives the resulting second order ordinary homogeneous differential equation,

$$m\ddot{w} + c\dot{w} + kw = f(t) = 0 \tag{3.8}$$

In the absence of external forcing an initial condition is imposed and the motion of the system takes either a nonoscillatory or oscillatory form in accordance with *D'Alembert's Principle*. The oscillatory form is characteristic of low values of damping typically encountered in *underdamped* aircraft so only this case will be considered [5].

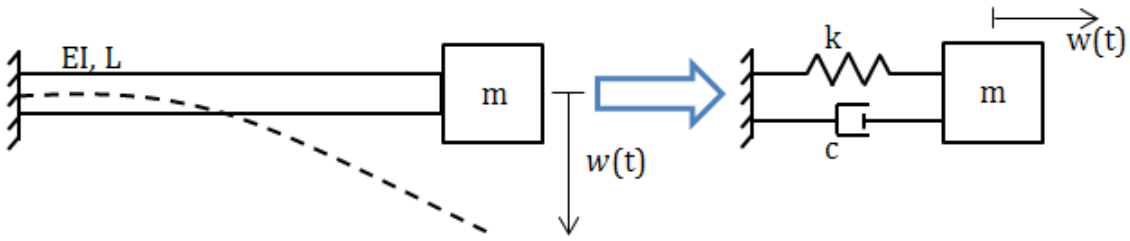

Figure 3.1 – Cantilever wing model and cooresponding SDOF system

Assuming free harmonic motion from equation 3.1 yields the characteristic quadratic equation of the SDOF cantilever beam model

$$\tilde{\lambda}^2 m + \tilde{\lambda} c + k = 0 \tag{3.9}$$

with the "characteristic solution" or eigenvalues of the of the system given as

$$\tilde{\lambda}_{1,2} = -\frac{c}{2m} \pm i\sqrt{\frac{k}{m} - \left(\frac{c}{2m}\right)^2}. \qquad 3.10$$

The eigenvalues can be non-dimensionalized in the form

$$\tilde{\lambda}_{1,2} = -\zeta\omega_n \pm i\omega_n\sqrt{1-\zeta^2} = -\zeta\omega_n \pm i\omega_d \qquad 3.11$$

where

$$\omega_n = \sqrt{\frac{k}{m}}; \qquad \omega_d = \omega_n\sqrt{1-\zeta^2}; \qquad \zeta = \frac{c}{2m\omega_n} = \frac{c}{c_{crit}}. \qquad 3.12$$

Here ω_n is the *natural circular frequency* of the system, ω_d is the *damped circular frequency* of the system, ζ is the *damping ratio* or damping normalized for critical nonoscillatory motion, c_{crit}[45]. The same characteristic approach applies to discrete multiple degree of freedom (MDOF) systems.

The difference between the natural circular frequency and the damped circular frequency is a function of the value ζ which typically ranges between 0.01 and 0.1 for the majority of real structures that undergo oscillatory motion. In the extreme case of $\zeta = 0.1$ the frequency of the damped system is nearly equal to that of the undamped system, $\omega_d = 0.99\omega_n$. Thus, in practice, the damping is ignored when determining the natural frequency and mode shapes of a system [45].

3.2.1. Natural frequency

The natural frequency occurs in an unforced case where the system acts independent of external forces including gravity. The natural frequency is only significant when assuming harmonic behavior. For MDOF systems, increases in the

mode number correspond to higher natural frequencies, and coupled vibration due to offset shear and mass centers results in unsorted distribution of the natural frequencies. For example, when coupled rotation and bending are considered, the first few usable (non-boundary condition) modes of the system may be intermixed between bending and torsion. Typically the lowest energy (frequency) mode is dominated by bending motion and the next lowest is dominated by torsion in a lightly coupled system where the shear and mass centers are only slightly offset.

3.2.2. Damping formulations

Damping represents the energy losses associated with a real system. The decreases in response amplitude in real systems are thus attributed to damping effects which typically convert mechanical and kinetic energy to thermal energy. However, damping is not necessarily an essential property of the structure itself, but often depends on the surrounding medium [46]. This inessential property of damping will be especially important with an inclusion of aerodynamic forces. Damping is typically described in two ways: *viscous damping* due motion within a fluid and *structural damping* due to internal friction within the material and joints.

3.2.2.1. Viscous damping

In many practical applications the damping forces are assumed to be viscous simply because the mathematical formulation for simple viscous damping is a linear proportion of the mass and stiffness of the structure know as *Rayleigh damping* [47]

$$D_{ij} = d_1 A_{ij} + d_2 E_{ij}. \quad 3.13$$

The scalar coefficients d_1 and d_2 are typically determined for a range of frequencies, $\omega_a - \omega_b$, but a SDOF system has only one frequency of interest so the formulation of the coefficients is not applicable and damping is typically expressed as a scalar value based on experience. With the addition of multiple discrete coordinates and corresponding frequencies, the coefficients are formulated [48] to satisfy desired damping ratios at the frequency extremes in the range of interest, ω_a and ω_b:

$$d_1 = \frac{2\omega_a\omega_b(\zeta_a\omega_b - \zeta_b\omega_a)}{\omega_b^2\omega_a^2}$$

$$d_2 = \frac{2(\zeta_a\omega_a - \zeta_b\omega_b)}{\omega_b^2 - \omega_a^2}. \quad 3.14$$

However, the desired damping ratios do not remain constant over the range of interest, so the formulation above leads to a conservative estimation. Viscous Rayleigh damping is applied at the system level and is applicable for any form of excitation.

3.2.2.2. Hysteretic damping

A simplified mathematical formulation of structural damping known as *hysteretic damping* relies on the dissipative force defined in equation 3.6 being proportional to the velocity and consequently the frequency of oscillation. Considering the SDOF cantilever model the harmonic motion $w(t)$ is described as function of the frequency, ω, and phase, ϑ, of the response,

$$w(t) = |w| \cos(\omega t - \vartheta). \quad 3.15$$

With a definition of the dissipative force as

$$-\frac{\partial \Im}{\partial \dot{w}} = -c\dot{w}, \tag{3.16}$$

the work energy dissipated is derived as follows[46]:

$$\begin{aligned} W_d &= \int c\dot{w}\, dz \\ &= \int_0^{2\pi/\omega} c\dot{w}^2\, dt \\ &= \int_0^{2\pi/\omega} c\omega^2 |w|^2 \sin^2(\omega t - \vartheta)\, dt \\ &= \pi c\omega |w|^2. \end{aligned} \tag{3.17}$$

As shown, the dissipative energy is dependent on the quadrature of the displacement, or physically at 90° phase to the displacement [5].

Experimental investigations have shown that the dissipative energy W_d in many metals is independent of frequency for the range of interest in aircraft systems [46, 47] so the damping $c(\omega)$ for the SDOF model must be represented as a frequency dependent function to cancel out the frequency dependence in equation 3.17,

$$c(\omega) = \frac{kg}{\omega}. \tag{3.18}$$

Considering only harmonic motion and using complex algebra in the frequency domain, the dissipative force becomes

$$\frac{\partial \Im}{\partial \dot{w}} = c\dot{w} = \frac{kg}{\omega}\dot{w} = ikgw, \tag{3.19}$$

where g is the damping coefficient or loss factor and $i\omega$ is equivalent to differentiation in the time domain[5]. If the dissipative force in equation 3.19 is substituted into equation 3.2, the new equation of motion for the SDOF system is

$$m\ddot{w} + ikgw + kw = f(t) = 0, \tag{3.20}$$

or rewritten as

$$m\ddot{w} + k(1 + ig)w = f(t) = 0 \tag{3.21}$$

with *complex stiffness* in place of the prescribed damping in equation 3.8. This frequency domain formulation of the equations of motion can only be used when the excitation is assumed to be harmonic and can be difficult to manipulate, but it is a classical method in the determination of aeroelastic behavior [6].

3.3. Application of the Finite Element Method

The goal of a structural dynamic analysis includes determination of the natural mode shapes and frequencies of an elastic structure in free unforced vibration. The FEM is well suited for this type of analysis since the mode shapes can be accurately derived for geometrically complex structures, such as channel beam sections commonly found in wing spars. The FE structural model is typically formulated as an eigensystem, where the eigenvalues and eigenvectors represent the natural frequencies and the mode shapes, respectively. The lowest eigenvalues correspond to the lowest characteristic frequencies of the physical system and are typically more interesting than the higher modes simply because the physical system tends to experience the lower modes as dominant vibration frequencies.

This section focuses on the FE derivation of the bending beam element and twisting torsion element used later for the dynamic analysis of lifting surfaces. The classical cubic beam element and linear torsion element are a natural foundation of the discussion and will lead to the derivation of the higher order quintic beam element and cubic torsion element capable of directly incorporating stress free conditions [49].

3.3.1. Classical element formulation

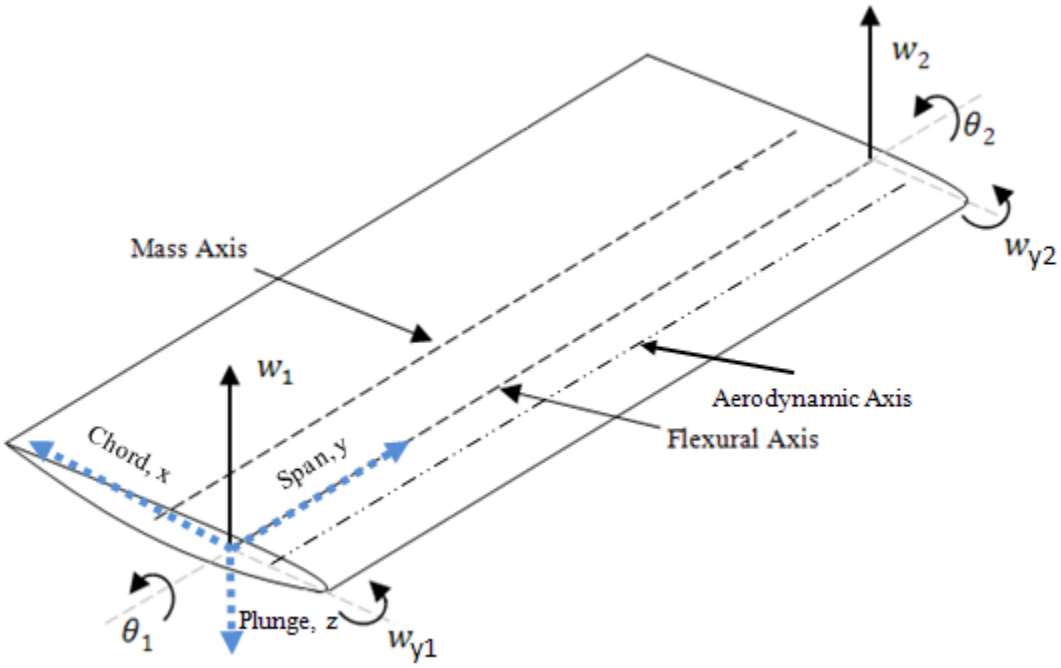

Figure 3.2 – Combined bending and torsion element

The classical uniform beam element of span length L_e, shown in Figure 3.2 joined with a linear torsion element, incorporates bending deflection w in one plane with no shear deformation where the strain potential energy in bending is

$$U = \frac{1}{2}\int_0^{L_e} EI\left(\frac{\partial^2 w}{\partial y^2}\right)^2 dy, \tag{3.22}$$

and the kinetic energy is

$$T = \frac{1}{2}\int_0^{L_e} \mu\left(\frac{\partial w}{\partial t}\right)^2 dy. \tag{3.23}$$

The flexural rigidity EI and mass per unit length μ are assumed constant across the beam element. It is assumed that the bending displacement can be expressed as a Hermite cubic polynomial as function of the spanwise coordinate, y [50]

$$w(y) = c_0 + c_1 y + c_2 y^2 + c_3 y^3, \tag{3.24}$$

where the unknown coefficients $c_0, \dots, c_3$ are determined based on the inter-element boundary conditions or nodal displacements and slopes, $w_y = \partial w/\partial y$, of a 2 node, 2 DOF per node element. An even better assumed shape could also satisfy the load (natural) boundary conditions.

Evaluating the mathematical coefficients c_j in terms of the physical nodal quantities gives the solution of the coefficients as functions of the local element coordinate η $(0 \le \eta \le 1)$ in the form of shape functions $N_1, \dots, N_4$

$$w = \boldsymbol{N}^T w_e. \tag{3.25}$$

The Hermite shape functions N_j are cubic polynomials in η [50]

$$\begin{aligned} N_1 &= 1 - 3\eta^2 + 2\eta^3 \\ N_2 &= L_e(\eta - 2\eta^2 + \eta^3) \\ N_3 &= 3\eta^2 - 2\eta^3 \\ N_4 &= L_e(-\eta^2 + \eta^3). \end{aligned} \tag{3.26}$$

Using equations 3.25 and 3.26, the strain energy and kinetic energy can then be respectively expressed as

$$U_{bending} = \frac{1}{2}\boldsymbol{w}_e^T\left[\int_0^{L_e} EI\left(N''N''^T\right)dy\right]\boldsymbol{w}_e, \tag{3.27}$$

$$T_{bending} = \frac{1}{2}\dot{\boldsymbol{w}}_e^T\left[\int_0^{L_e} \mu(NN^T)dy\right]\dot{\boldsymbol{w}}_e. \tag{3.28}$$

Using a transformation from y to η the resulting classic uniform beam element stiffness and mass matrices are given as [9]

$$k_e = \frac{EI}{{L_e}^3}\begin{bmatrix} 12 & 6L_e & -12 & 6L_e \\ 6L_e & 4{L_e}^2 & -6L_e & 2{L_e}^2 \\ -12 & -6L_e & 12 & -6L_e \\ 6L_e & 2{L_e}^2 & -6L_e & 4{L_e}^2 \end{bmatrix}, \tag{3.29}$$

$$m_e = \frac{\mu L_e}{420}\begin{bmatrix} 156 & 22L_e & 54 & -13L_e \\ 22L_e & 4{L_e}^2 & 13L_e & -3{L_e}^2 \\ 54 & 13L_e & 156 & -22L_e \\ -13L_e & -3{L_e}^2 & -22L_e & 4{L_e}^2 \end{bmatrix}. \tag{3.30}$$

The torsion element is formulated in a similar manner assuming linear shape functions to account for the nodal torsional displacements

$$\begin{aligned} N_1 &= 1-\eta \\ N_2 &= \eta, \end{aligned} \qquad \text{where} \qquad \theta = \boldsymbol{N}^T\theta_e. \tag{3.31}$$

The shape functions only need be once differentiable in the equations of motion

$$U_{Torsion} = \frac{1}{2}\boldsymbol{\theta}_e^T\left[\int_0^{L_e} GJ\left(N'N'^T\right)dy\right]\boldsymbol{\theta}_e, \tag{3.32}$$

$$T_{Torsion} = \frac{1}{2}\dot{\boldsymbol{\theta}}_e^T\left[\int_0^{L_e} \frac{\mu I_0}{A_r}(NN^T)dy\right]\dot{\boldsymbol{\theta}}_e. \tag{3.33}$$

The explicit uniform torsion stiffness and mass element matrices are given as [9]

$$k_e = \frac{GJ}{L_e}\begin{bmatrix} 1 & -1 \\ -1 & 1 \end{bmatrix}, \qquad m_e = \frac{\mu I_0 L_e}{6A_r}\begin{bmatrix} 2 & 1 \\ 1 & 2 \end{bmatrix}. \tag{3.34}$$

Here, GJ is the torsional rigidity, I_0 is the polar moment of inertia and A_r is the cross sectional area reference dimension based on the aerodynamic mean chord length. The reference area is required to maintain consistent units of energy.

The Hermite cubic polynomial bending element and linear torsion element are commonly used in many structural analyses especially in beam-like representations of aeroelastic structures. Three-dimensional aeroelastic behavior is replicated by a combination of bending elements to account for the bending in plunge and sway, a torsion element to account for pitch and an axial extension element. The result is 12x12 element stiffness and mass matrices. However, the axial extension is often negligible without thermal considerations and the bending sway in the perpendicular direction is often negligible due to low drag force relative to lift, and high sway stiffness. Additionally, the characteristic vibrational behavior of these neglected modes is often not manifest in experimental behavior [31]. So the remaining modes of interest result in the combined 6x6 *modified beam element* shown in

Figure 3.2. The explicit combination of the plunge bending and torsion elements is given in classical form as

$$k_e = \begin{bmatrix} 12\frac{EI}{{L_e}^3} & 6\frac{EI}{{L_e}^2} & 0 & -12\frac{EI}{{L_e}^3} & 6\frac{EI}{{L_e}^2} & 0 \\ 6\frac{EI}{{L_e}^2} & 4\frac{EI}{L_e} & 0 & -6\frac{EI}{{L_e}^2} & 2\frac{EI}{L_e} & 0 \\ 0 & 0 & \frac{GJ}{L} & 0 & 0 & -\frac{GJ}{L_e} \\ -12\frac{EI}{{L_e}^3} & 6\frac{EI}{{L_e}^2} & 0 & 12\frac{EI}{{L_e}^3} & -6\frac{EI}{{L_e}^2} & 0 \\ 6\frac{EI}{{L_e}^2} & 2\frac{EI}{L_e} & 0 & -6\frac{EI}{{L_e}^2} & 4\frac{EI}{L_e} & 0 \\ 0 & 0 & -\frac{GJ}{L_e} & 0 & 0 & \frac{GJ}{L_e} \end{bmatrix} \quad 3.35$$

$$m_e = \frac{\mu L_e}{420}\begin{bmatrix} 156 & 22L_e & 0 & 54 & -13L_e & 0 \\ 22L_e & 4{L_e}^2 & 0 & 13L_e & -3{L_e}^2 & 0 \\ 0 & 0 & 140\frac{I_0}{c^2} & 0 & 0 & 70\frac{I_0}{c^2} \\ 54 & 13L_e & 0 & 156 & -22L_e & 0 \\ -13L_e & -3{L_e}^2 & 0 & -22L_e & 4{L_e}^2 & 0 \\ 0 & 0 & 70\frac{I_0}{c^2} & 0 & 0 & 140\frac{I_0}{c^2} \end{bmatrix} \quad 3.36$$

The mass matrix above only accounts for the kinetic energy of a specific beam structure moving in pure plunge and pitch.

3.3.2. Higher order beam finite element

The two node Hermite cubic beam bending element gives exact nodal displacements and slopes, but poor internal loading representation since the moment and shear are dependent on the second and third derivatives of the solution, respectively. The cubic polynomial can be raised to a fifth order or quintic polynomial to accurately capture the internal loading and the displacements with fewer elements. Thus, the quintic interpolation essentially gives the exact solution for distributed loading on a cantilever beam. Additionally, the linear torsion element is only accurate when neglecting shear effects. The shear can be represented by a warping component of twist that is dependent on the second derivative of the linear elastic torsion. Thus, a cubic torsion element is desirable.

The quintic beam element can be formulated for a three node element in terms of the element deflection and slope. The Hermite quintic polynomial shape functions in η are then given as [50]

$$\begin{aligned} N_1 &= 1 - 23\eta^2 + 66\eta^3 - 68\eta^4 + 24\eta^5 \\ N_2 &= L_e(\eta - 6\eta^2 + 13\eta^3 - 12\eta^4 + 4\eta^5) \\ N_3 &= 16\eta^2 - 32\eta^3 + 16\eta^4 \\ N_4 &= L_e(-8\eta^2 + 32\eta^3 - 40\eta^4 + 16\eta^5) \\ N_5 &= 7\eta^2 - 34\eta^3 + 52\eta^4 - 24\eta^5 \\ N_6 &= L_e(-2\eta^2 + 5\eta^3 - 8\eta^4 + 4\eta^5) \end{aligned} \tag{3.37}$$

The explicit quintic element stiffness and mass matrices are given in the appendix for reference.

3.4. Characteristic Modeling

The assembly of the stiffness and mass elements into the respective system structural stiffness matrix $\boldsymbol{E}$ and system inertia matrix $\boldsymbol{A}$ gives the total system behavior with respect to the discrete coordinates of the system. The characteristic dynamic behavior can then be modeled using [46]

$$[\boldsymbol{E} - \lambda_j \boldsymbol{A}]\phi_j = 0 \tag{3.38}$$

where the eigenvalue λ_j represents the natural frequency and the eigenvector ϕ_j represents an arbitrary displacement profile or mode of the discrete coordinates. The solution of the equation is achieved by setting the determinate of the brackets equal to zero. The resulting nontrivial solution is a vector of real eigenvalues of length *n* that describe the natural vibrations frequencies of the system. The contribution of the DOFs of interest can then be investigated by plotting the mode

shapes of each DOF with respect to the other DOF through relative scaling scheme, such as maximum unit displacement used herein.

3.5. Free Vibration of Coupled Multiple Degree of Freedom Systems

The free vibration analysis of high aspect ratio wing structures is a natural application of the modified beam element where the wing structure is equated to a long slender beam capable of bending and torsion. For many classical beam cross sections, such as I-beams or hollow square beams the cross section is doubly symmetric about both horizontal and vertical axes. This double symmetry leads to an uncoupling of bending and torsional motion. However, even in simple classical wing structures, such as NACA 4-series airfoils, the cross section has only single symmetry or no symmetry in the case of NACA 2412 airfoil. This loss of cross-sectional symmetry leads to a coupling effect of bending and torsional motion due to an offset of the center of gravity and the center of shear some distance $e_m$referred to as *inertial eccentricity*. The resulting coupled equations of motion are dynamically coupled but elastically uncoupled. The coupled elastic potential energy including the effects of the geometric warping C_w is given as [25]

$$U = \frac{EI}{2}\int_0^L \left(\frac{\partial^2 w}{\partial y^2}\right)^2 dy + \frac{GJ}{2}\int_0^L \left(\frac{\partial \theta}{\partial y}\right)^2 dy + \frac{EC_w}{2}\int_0^L \left(\frac{\partial^2 \theta}{\partial y^2}\right)^2 dy \qquad 3.39$$

and the coupled kinetic energy is given as

$$T = \frac{\rho_m A_r}{2}\left[\int_0^L \left(\frac{\partial w}{\partial t}\right)^2 dy + 2e_m \int_0^L \frac{\partial w}{\partial t}\frac{\partial \theta}{\partial t} dy\right] + \frac{\rho_m I_o}{2}\int_0^L \left(\frac{\partial \theta}{\partial t}\right)^2 dy \qquad 3.40$$

The terms ρ_m and A_r are the mass density and reference area respectively, and they are given as such to maintain consistent energy formulation. An alternative formulation as mentioned in section 3.3.1 is the mass per unit length, μ. Both formulations are commonly used in classical analysis.

3.5.1. Natural frequency and mode shape validation

The free vibration natural frequencies and mode shapes of inertial eccentric beams are the precursor to an inclusion of aerodynamic effects. Accurate application of the fundamental or lower structural modes requires a verification of the frequencies and mode shapes. Thus the coupled vibration FEM model is compared to a published case study listed in Table 3.1. The classic cubic interpolation is consistently used for beam bending and torsion and the results are compared to the higher order quintic interpolation to show convergence on the excepted values.

Table 3.1 – Case study material and geometry data

Model	EI [Nm^2]	GJ [Nm^2]	ρ_m [kg/m^3]	A_r [m^2]	e_m [m]	I_0 [m^4]	L [m]
Cantilever Wing[39, 51]	9.75 x 10^6	9.88 x 10^5	42.8	0.836 (=b^2)	0.18	0.202	6

The cantilever square wing example presented by Banerjee [51] is the classical model used for the analytical prediction of flutter characteristics [39]. The

first two fundamental frequencies are most important in aeroelastic analysis since the lowest modes are typically less damped and more susceptible to physical aerodynamic effects. The first two fundamental frequencies are 49.6rad/s and 97.0rad/s which agree completely with the FEM mode shape plots in Figure 3.3. The first plot in the figure shows the use of one element with cubic interpolation and the second uses five elements. The one element case does not produce the exact fundamental frequencies and mode shapes, but the five element case does essentially produce the exact solution after a monotonic convergence with the inclusion of more elements. The cubic interpolation does essentially converge to the exact result with the use of only two elements, but five elements are used to maintain consistency with the later aeroelastic formulation, which requires five cubic elements for convergence.

The quintic interpolation of the example data with three nodes per element is shown in Figure 3.4. The fundamental frequencies and mode shapes are essentially achieved with only one quintic element, which is a clear advantage over the cubic interpolation. The behavior of the mode shape plots for each respective mode is indicative of the individual contributions of the uncoupled motions. The first mode at 49.6 rad/s is dominated by the bending motion as shown by the relative scaling of the maximum characteristic displacement at the tip (right side). The second mode is dominated by torsion for the same reason. Thus, the two lower modes of this model are the primary suspects for consideration of aeroelastic influence since a combination of bending and torsion in phase results in dynamic flutter.

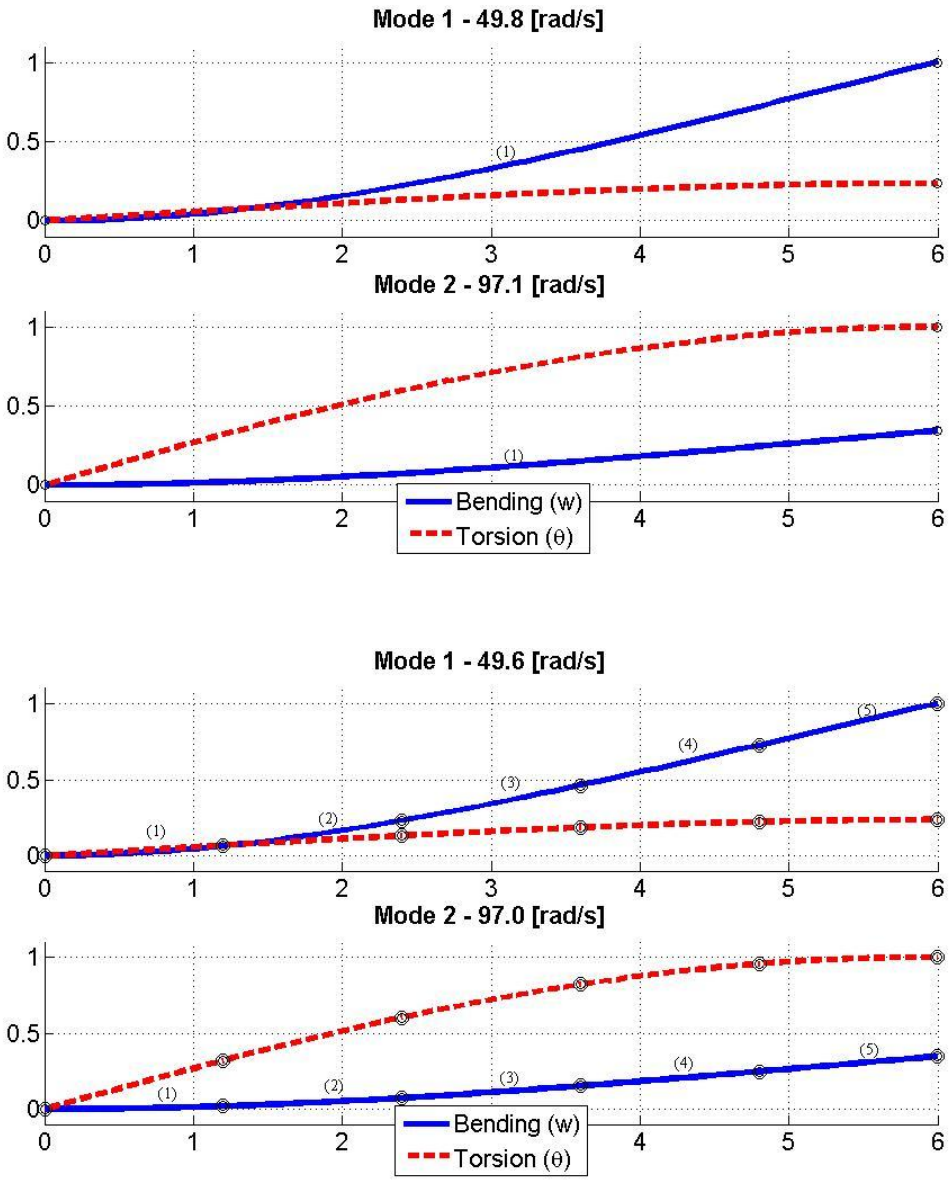

Figure 3.3 - Coupled bending and torsion fundamental natural frequencies and mode shapes of case study data – Cubic interpolation FEM, 2 nodes per element, 1 and 5 elements

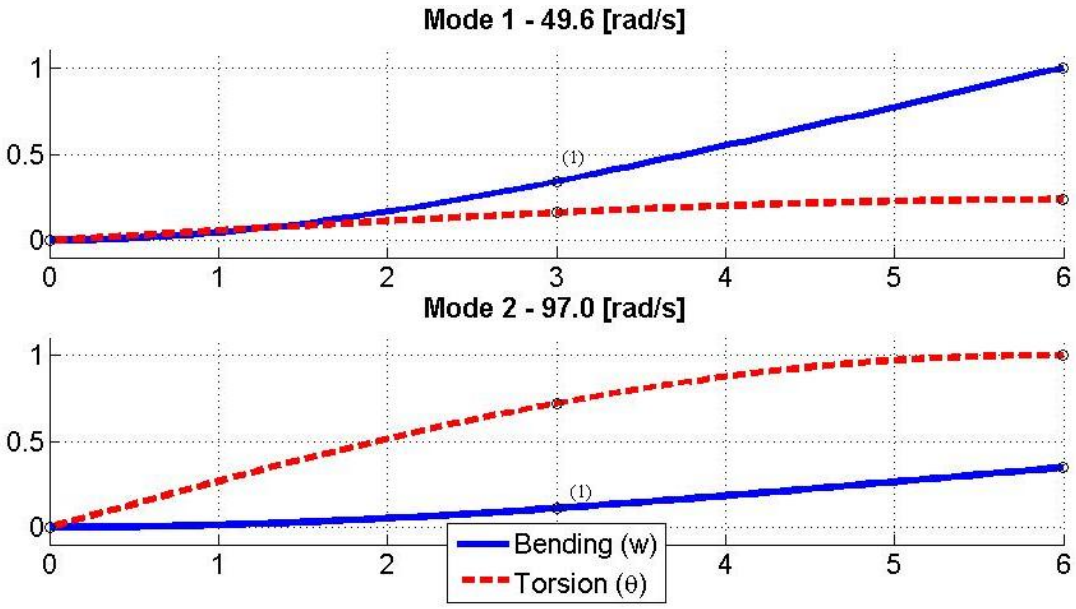

Figure 3.4 – Coupled bending and torsion fundamental natural frequencies and mode shapes of case study data – Quintic interpolation FEM, 3 nodes, 1 element

Chapter 4

Static Aeroelasticity

Static aeroelasticity is the study of the interaction of aerodynamic loads and elastic flexibility independent of inertial time varying loads. The lifting load model of *steady aerodynamics* is used since acceleration based forces are eliminated from the equations of motion, and the loading is only a function of the local incidence of the lifting surface to the airstream [20]. The loading is assumed to cause small elastic deformation which changes the lifting characteristics of the surface enough to alter the loading until an equilibrium condition is reached. If the aerodynamic loading overcomes the elastic restoring moment before equilibrium is reached at a cruise condition, the structure experiences unbounded displacement in a phenomenon known as *divergence* [5].

The structural stiffness is much more important than the strength in aeroelastic considerations, and the torsional stiffness is the primary divergence mode [2, 7]. The static aeroelastic models used will incorporate the flexible torsion

of a structure combined with the loading distribution of a lifting surface. The geometry configurations of the lifting surface and structural model, such as varied sweep and taper, also significantly affect the lifting and stability characteristics of the model and will be considered. Static aeroelasticity is a component of full dynamic aeroelasticity, and is a logical precursor to a full appreciation of dynamic aeroelasticity.

4.1. Modeling and Prediction

4.1.1. Model nomenclature

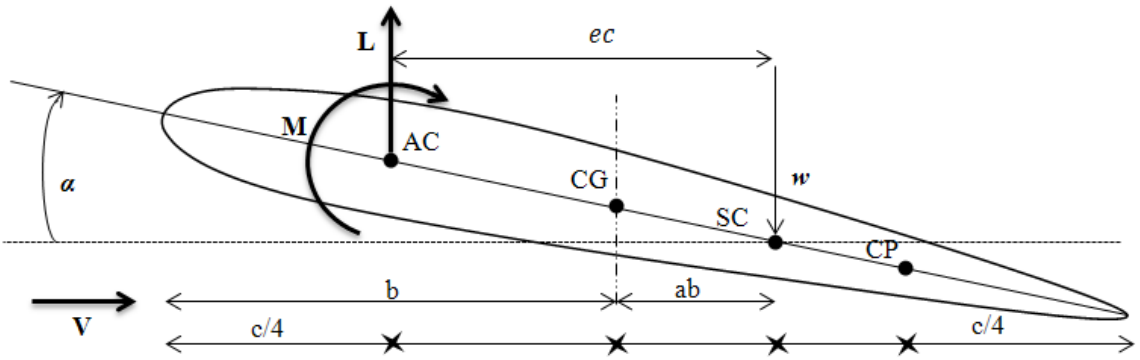

Figure 4.1 – 2 DOF bending and torsion airfoil model

A full aeroelastic model includes aerodynamic, inertial and structural features, but the inertial components are only mentioned and not considered in static aeroelastic analysis. Thus, an aerodynamic load and elastic deformation model will be used to study bending and twisting effects. An aerodynamic fundamentals model with pitch and plunge DOFs allows for sufficient analysis of the relationship between aero loading due to lift and drag and the resulting deformation [52].

Determination of the terminology of the model is critical to proper application of the model dynamics. The standard reference dimension of airfoil models is the measure from the leading edge to the trailing edge called the chord, c. However, the half chord, b, is used interchangeably as a reference dimension. The point origin of many airfoil models is the leading edge, but the origin used for the two DOF model shown in Figure 4.1 is the elastic *shear center* (SC) measured a distance ab from the mid chord. A force applied at this point will cause pure plunge and no pitch, and a moment will cause pure pitch and no plunge. This reference and origin configuration is typical of many classical aeroelastic derivations[5–7].

The point origin is used to gauge the displacement of the structure. The plunge term is represented by w, measured positive down from the SC origin. The pitch term is represented by α, measured positive leading edge up about the SC origin. The pitch term or *angle of attack* is combination of the rigid body incidence and the elastic torsion of the airfoil about the SC [3]

$$\alpha \equiv \alpha_r + \theta. \tag{4.1}$$

The appropriate extension of the SC to a three-dimensional wing of span, s, is the line of shear centers called the *flexural axis* (FA). This is the general line of points where an applied load causes pure plunge or pitch. The weight of the structure acts about the *center of gravity* (CG) usually located at the mid chord, with the *mass axis* (MA) representing the wing equivalent. The wing axis representations are shown in

Figure 3.2. If the MA and FA are offset, the bending and torsion modes are coupled in the inertia terms.

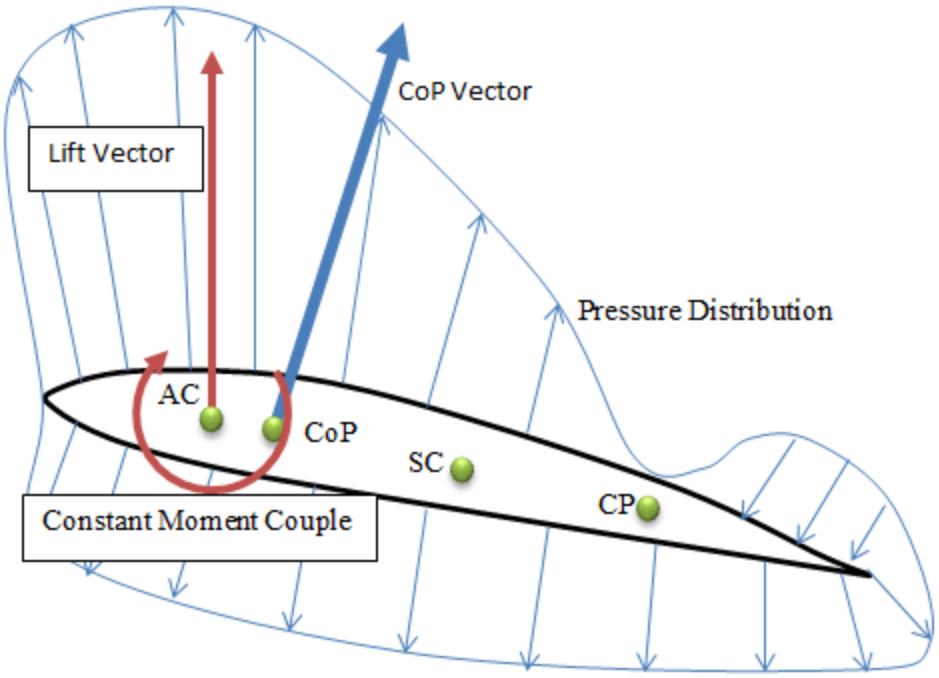

Figure 4.2 – Pressure distribution and reference points on an airfoil surface

The lift distribution over an airfoil is accurately described by a non-uniform chordwise pressure distribution, and the effective *center of pressure* (CoP) is the location where the pressure distribution can be idealized as a force vector. This location varies with a change in the pressure in distribution, so it is not used in this analysis, see Figure 4.2. Alternatively, the *aerodynamic center* (AC) is the point on the airfoil where pitching moment coefficient does not change with flight conditions and it is measured a distance *ec* from the SC termed *aerodynamic eccentricity*. For symmetric thin airfoils, this point is exactly the quarter chord $\left(\frac{c}{4}\right)$, and general airfoil shapes differ only slightly. The orthogonal lift and drag vectors act about the AC and vary in magnitude depending on the flight conditions, but the moment couple is constant or zero for thin symmetric airfoils. The lift then creates a moment about

the SC with a moment arm of *ec.* The extension to three-dimensional wings is the axis of aerodynamic centers (AA). Another significant reference is the *control point* (CP) located at the three-quarter chord $\left(\frac{3c}{4}\right)$, which satisfies the boundary of flow tangency necessary for the inviscid flow assumption [20].

4.2. Steady Aerodynamics

The loading of a lifting surface is the primary contribution of the aerodynamics to the ternary flutter problem, so a formulation of predictable loading is important. The *steady aerodynamic* formulation of loading assumes that the velocity of the inviscid and incompressible flow field around a lifting surface is constant in time; thus, this formulation is appropriate for a static analysis.

The forces of the steady flow can be expressed in terms of dimensionless quantities. The *dynamic pressure*

$$q = \frac{1}{2}\rho V^2, \tag{4.2}$$

relates the atmospheric density, ρ, and flow velocity, V, to the pressure dimensional quantity, q. The dimensionless loading coefficients are then expressed as spanwise external forcing over the dynamic pressure and a reference dimension in the form

$$C_L = \frac{Lift}{q*c*span}, \qquad C_M = \frac{Pitching\ Moment}{q*c^2*span}. \tag{4.3}$$

The drag force is not considered since the chordwise bending or sway is small compared to the spanwise bending due to high chordwise stiffness.

Considering only attached sub stall flow, the loading response is linearly proportional to the incidence angle and is known as the airfoil *lift curve slope*

$$a_1 = \frac{\partial C_L}{\partial \alpha}, \tag{4.4}$$

which is idealized as 2π for thin, symmetric two-dimensional airfoils in incompressible flow [53, 54]. For a finite three-dimensional wing, the lifting load can be expressed as the total loading of each two-dimensional airfoil strip over the span [5] in the form of external forcing similar to equation 3.7

$$L_{total} = q \int_{span} c a_1 \alpha(y) dy \tag{4.5}$$

$$M_{total} = q \int_{span} e c^2 a_1 \alpha(y) dy. \tag{4.6}$$

In general, the chord and lift curve slope can vary with the span as a function of y so the terms are retained inside the spanwise integral. For a rectangular untapered wing, the terms are constant across the span.

The *strip theory* of airfoils, expressed for a continuous wing in equations 4.5 and 4.6, models the finite wing as a series of spanwise strips with lift proportional to the local incidence of the strip. This theory is well suited for discretization and direct coupling to a finite element modified beam structural model, so it will be the primary focus of the loading calculation.

4.2.1. Strip theory discretization

The strip theory can be used in conjunction with a FEM beam model in a discrete structure to calculate the loading on each individual beam element. The discrete representation of the loading per individual strip is of the form [5]

$$L_{ae} = qca_1\alpha(y_{ae})\Delta y_{ae} \tag{4.7}$$

$$M_{ae} = qec^2a_1\alpha(y_{ae})\Delta y_{ae} \tag{4.8}$$

where the subscript ae denotes the individual aerodynamic element of interest out of n_{ea} strips. The density of the aerodynamic elements n_{ea} can differ from the density of the structural elements n_e, but the densities will be consistent for an application of strip theory to beams elements. The term Δy_{ae} is the width of the strip with the spanwise reference in the center of the strip. The lift curve slope is potentially modified by a change in atmospheric flow conditions most notably the compressibility of the flow at high subsonic Mach (Ma) number [54]

$$0.3 \leq Ma = {}^{Velocity}/_{Speed\ of\ Sound} \leq 0.7. \tag{4.9}$$

The lift curve slope is then given by the Prandtl-Glauert rule valid in the range specified above

$$a_{1c} = \frac{a_1}{\sqrt{1 - Ma^2}}. \tag{4.10}$$

The modified, compressible lift curve slope is a suitable replacement for the ideal value of airfoils when considering the loading on real wing structures. The total spanwise loading is then given by the sum of the individual aerodynamic elements

$$L_{total} = \sum_{ae=1}^{n_{ea}} L_{ae}, \qquad M_{total} = \sum_{ae=1}^{n_{ea}} M_{ae}. \tag{4.11}$$

4.3. Static Divergence

Divergence is the phenomenon of unbounded deflection caused by insufficient structural stiffness. Wing torsional divergence is the most common instability, so a flexible torsional 2 DOF wing model will be developed to demonstrate the driver of the instability.

4.3.1. SDOF Model

The SDOF case of pitch only deflection is a simple case used to demonstrate the wing divergence condition. Consider a two-dimensional airfoil model with a torsion spring K_T located at the SC. The plunge DOF is eliminated leaving the following neutral stability condition with applied pitching moment

$$K_T\theta = qec^2a_{1c}(\alpha_r + \theta). \tag{4.12}$$

Rearranging for the elastic torsion θ gives a simple representation of the aeroelastic equation in the form

$$(K_T - qec^2a_1)\theta = qec^2a_{1c}\alpha_r. \tag{4.13}$$

The addition of the structural and aerodynamic terms on the left hand side of the equation is the effective aeroelastic stiffness, which decreases as the dynamic pressure increases. The effective stiffness can be represented as the rate of change

of the total moment about the shear center with respect to the elastic torsional angle θ [10]

$$\frac{\partial M}{\partial \theta} = K_{effective} = K_T - qec^2 a_{1c}. \tag{4.14}$$

Solving for the elastic torsion gives a closed form equation in terms of the rigid airfoil incidence

$$\theta = \frac{qec^2 a_{1c}}{(K_T - qec^2 a_{1c})} \alpha_r. \tag{4.15}$$

The airfoil diverges when the denominator of equation 4.15 goes to zero. The flight condition that satisfies the divergence criteria is called the *divergence dynamic pressure*

$$q_D = \frac{K_T}{ec^2 a_{1c}}. \tag{4.16}$$

The neutral stability or divergence is a special case only considering the deflection dependent external aero forces and the internal structural forces. This special case is self-equilibrating and non-unique, thus it is uncontrollable [55]. A plot of non-dimensional elastic torsional divergence is shown in Figure 4.3 as function of the flight condition up to divergence [3]. The elastic torsion equals the rigid incidence at half the divergence dynamic pressure, effectively doubling the total pitch angle. The torsion then grows exponentially as the flight condition approaches divergence.

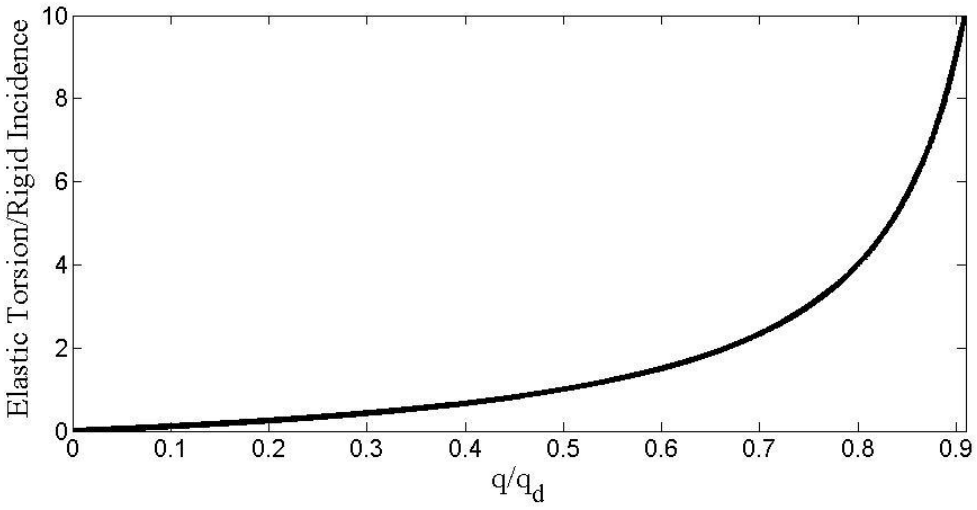

Figure 4.3 –Torsional divergence of SDOF spring model

4.3.2. FEM model

The aeroelastic motion of a MDOF body can be idealized using differential equations and subsequently modeled using FE analysis techniques. The torsion only motion can be modeled using an ideal square wing with constant aerodynamic eccentricity. The aerodynamic loads act along the AA, which are offset from the FA. Only the torsion is modeled, but the wing will also bend under the application of an aerodynamic load.

The wing twist deflection is characterized by a linear assumed displacement. Considering a consistent discrete representation of the wing strip and torsion structure with $n_{ea} = n_e = 2$ nodes per strip/element, the interpolation functions are given in equation 3.31 and the torsion element vector θ_e can be replaced by the generalized coordinate vector φ. The explicit structural stiffness element matrix is

given in equation 3.34, and the aeroelastic strip length s_{ae} replaces the structural element length L_e.

The spanwise couple due to the lift offset from the FA is given by equation 4.8. The incremental work done by the couple over an aerodynamic element is the integral of the spanwise force per equation 3.7

$$\delta W_{ae} = \int_0^{s_{ae}} qec^2 a_{1c}(\alpha_r + N\varphi^T)\,\delta(N^T\varphi)dy. \tag{4.17}$$

Rearranging the loading term gives the aerodynamic element matrix integral

$$\delta W_{ae} = \left[\int_0^{s_{ae}} qec^2 a_{1c}(\alpha_r N^T + NN^T\varphi)\,dy\right]\delta\varphi \tag{4.18}$$

Using Lagrange's equations gives the explicit aeroelastic formulation for a 2 node aeroelastic torsion model

$$\frac{GJ}{L_{ae}}\begin{bmatrix}1 & -1\\ -1 & 1\end{bmatrix}\begin{bmatrix}\varphi_1\\ \varphi_2\end{bmatrix} = \frac{1}{2}qec^2 a_{1c}s_{ae}\alpha_r\begin{bmatrix}1\\ 1\end{bmatrix} + \frac{1}{6}qec^2 a_{1c}s_{ae}\begin{bmatrix}2 & 1\\ 1 & 2\end{bmatrix}\begin{bmatrix}\varphi_1\\ \varphi_2\end{bmatrix} \tag{4.19}$$

The aerodynamic stiffness term $\boldsymbol{C}$ on the far right hand side of the equation is grouped with the structural stiffness on the left hand side of the equation. The fixed root boundary condition is enforced on the first generalized coordinate to give an explicit formulation of the remaining generalized coordinates in terms of the rigid incidence. The second generalized coordinate in the this case corresponds to the outboard tip torsional displacement

$$\theta_{tip} = \varphi_2 = \frac{3qec^2{a_{1c}}{s_{ae}}^2}{6GJ - 2qec^2{a_{1c}}{s_{ae}}^2}\alpha_r, \tag{4.20}$$

which is identical to the assumed shaped solution given by Wright [5]. The divergence dynamic pressure is derived from the neutral stability as before

$$q_D = \frac{3GJ}{ec^2{a_{1c}}{s_{ae}}^2}. \tag{4.21}$$

The resulting lift distribution is the primary focus of an aircraft design engineer. At the divergence limit, the loading tends to infinity, but structural failure will first occur based on the structural integrity. A common aerodynamic reference for the structural load limit is a *V-n* diagram, which has a $\bar{q}$ limit at some high dynamic pressure as shown on the right hand side of Figure 4.4. This limit is typically an aerothermoelastic limit, but when temperature effects are neglected the limit reduces to an aeroelastic limit, which is predictable by static analysis [3, 56].

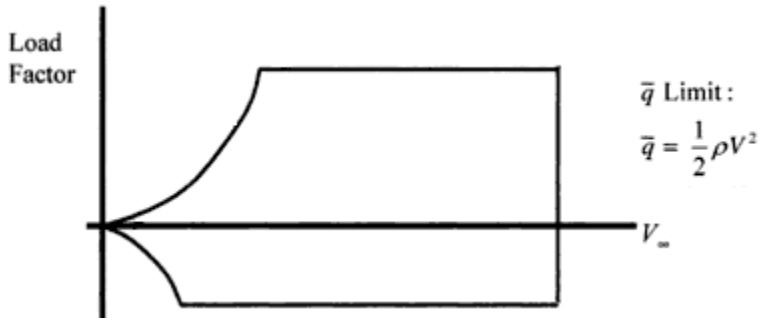

Figure 4.4 – V-n loading limit diagram example [54]

Chapter 5

Dynamic Aeroelasticity

The problem of flutter is extremely important in the design and development of aircraft structures. Many stiffness based criteria in airframes are based on flutter requirements [3], which also determine airworthiness and maintenance schedules [56]. Considering Figure 1.1, the structural dynamic characteristics of flight vehicles covered in Chapter 3 coupled with the aeroelastic loading and effects covered in Chapter 4 produce a unique phenomenon described by *dynamic aeroelasticity*. In static aeroelastic analysis, the aerodynamic surfaces are assumed to be in a steady condition so the forces acting on the surfaces are constant in time leading to divergence criteria. The inclusion of dynamic effects requires a consideration of the outcome of changing circulation and wake acting upon a moving airfoil described as *unsteady* effects [5]. The inclusion of unsteady aerodynamic effects leads to a

meaningful representation of the characteristics of aeroelastic flutter, but presents a complicated analysis even with linearized aerodynamics and clean lifting surfaces.

There are many dynamic aeroelastic phenomena that could be considered but flutter is arguably the most important of all the aeroelastic phenomena and is the most difficult to predict [6]. It is an unstable self-excited vibration in which the structure extracts energy from the air stream and often results in catastrophic structural failure. Lifting surface flutter is most often encountered in aircraft systems and is the primary focus of aeroelastic design. Classic *binary flutter* occurs on lifting surfaces when the motion of two modes of vibration couple unfavorably [5] as shown in Figure 2.2. The bending and torsion model of an airfoil strip is well suited to account for binary flutter, but there are cases when more than two modes can cause flutter in wing elastic structures so multimodal mathematical models are employed in industry prediction techniques [15].

In this chapter, a binary flutter 2 DOF model is developed with unsteady strip theory aerodynamics and elastic bending and torsional structural dynamics. The mathematical representation of the analysis is a linear set of ordinary differential equations with aerodynamic external forcing linearly proportional to the system response. The equations of motion are used in an *eigenvalue problem*, and the stability characteristics are investigated in terms of the eigenvalues. The 2 DOF case is then expanded to a MDOF FEM case considering only lowest modal interactions.

5.1. Unsteady Aerodynamics

The derivation of lifting loads with the *strip theory* of aerodynamics was covered in Chapter 4 for two-dimensional inviscid, compressible flow over a thin airfoil undergoing small displacement. Although there are obvious deficiencies with a linearized, two-dimensional theory the most significant drawback is that it neglects unsteady effects critical to accurate flutter analysis. The development of unsteady aerodynamic theories is a classical and ongoing endeavor, which is simplified when one assumed harmonic motion *a priori* [3]. The harmonic assumption then naturally leads to a frequency domain analysis of unsteady airfoil response in lieu of a time domain analysis since the motion at the stability boundary modeled in the frequency domain is of more interest.

5.1.1. Quasi-steady aerodynamics

The steady aerodynamic models employed in Chapter 4 relied on the assumption of an airfoil or wing fixed relative to the air flow with the resulting forces and moments remaining constant in time. In general, the forces and moments vary with time as the airfoil moves. One simple approach for the estimation of general aeronautical forcing worth mentioning is the idea of *quasi-steady* aerodynamics [5]. The basic assumption is that the time dependent motion of the airfoil behaves with characteristics equivalent to a steady moving airfoil at that instant of time. The result is an instantaneous change in loading when the flight conditions, such as pitch and plunge, are changed. However, the lack of frequency

dependence means that the response is exactly in phase with the loading, when actually the perturbed response lags steady-state value.

One method for modeling the response lag with quasi-steady aerodynamic theory is *Wagner's function,* which models the lag in response due to indicial forcing as a function of non-dimensional time $\tau = {}^{Vt}/_{b}$. Wagner's function is usually approximated for incompressible flow as [20]

$$\boldsymbol{\Phi}(\tau) = 1 - \frac{2}{4+\tau}, \tag{5.1}$$

and the change in lift per unit span of an airfoil is then expressed as

$$\Delta L = \frac{1}{2}\rho V^2 (2b)(2\pi)\Delta\alpha\boldsymbol{\Phi}(\tau). \tag{5.2}$$

The plot in Figure 5.1 shows the time domain lag of the lift force calculated using equations 5.1 and 5.2 compared to the pure quasi-steady force. The quasi-steady lifting force occurs instantly once the wind is turned on, but the unsteady Wagner forcing starts at half the quasi-steady value and lags nearly 15 semi-chords before reaching a steady state value. The combined effect of this lagging in an oscillating airfoil can be expressed as a convolution of each change in flight condition if the time domain solution is desired. The quasi-steady aero model is a traditional technique (see Table 2.1) for aeroelastic modeling, but has obvious drawbacks. The quasi-steady lift model is also typically standard for undergraduate aerodynamics texts [4, 53, 54].

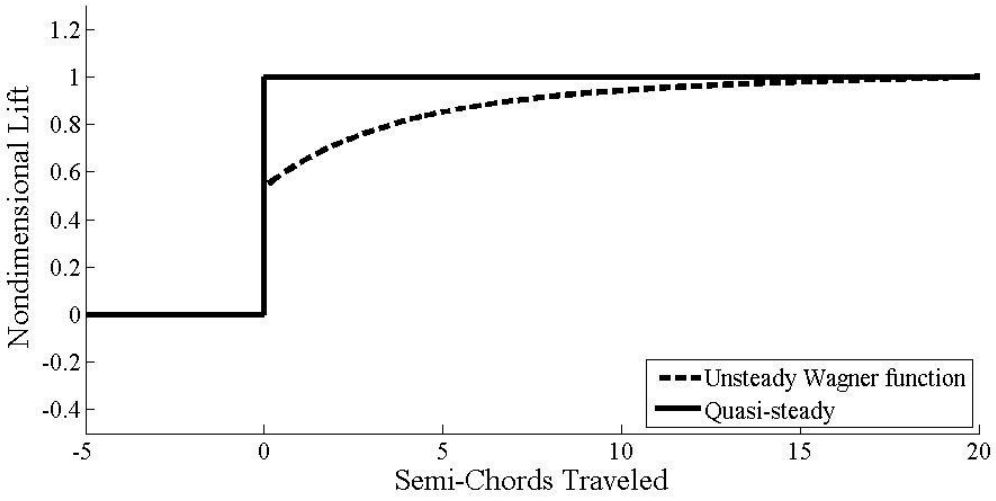

Figure 5.1 – Wagner function and the effect of sudden change in incidence

5.1.2. Harmonic Motion

The harmonic motion assumption is a much more powerful tool in aeroelastic analysis that can capture frequency dependent effects allowing for proper flutter stability modeling [8]. As the frequency of the airfoil motion changes the *phase lag* and *magnitude* of the response also change. The response can be formulated as a function of the dimensionless *reduced frequency* parameter [6, 20],

$$k = \frac{\omega b}{V}. \qquad 5.3$$

This is the number of circular oscillations of the airfoil in the time taken for the flow to cross one semi-chord b of the airfoil. The reduced frequency parameter is similar to the Strouhal number of fluid mechanics used to measure the vortex shedding of oscillating bodies.

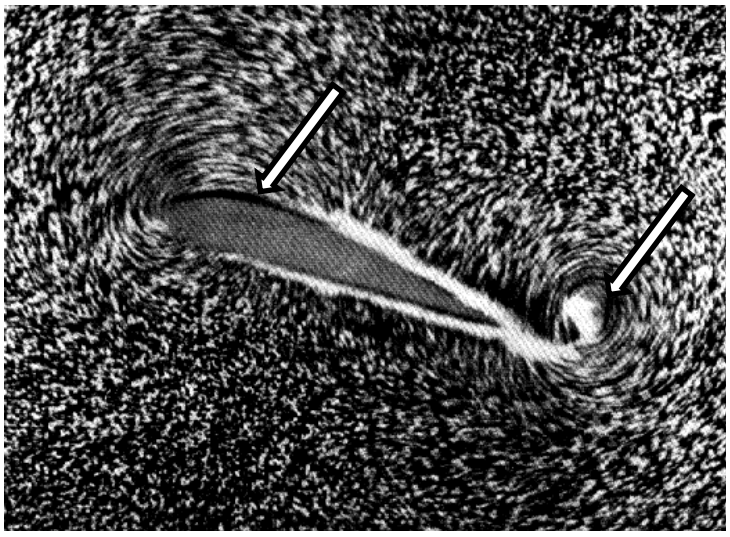

Figure 5.2 – Vortex generation of a moving airfoil [57]

In general, the loading on an oscillating airfoil is due to the periodic shedding of trailing edge vortices. As shown in Figure 5.2, the airfoil incidence and the fluid motion causes a trailing or *shed vortex* to form at the sharp trailing edge. As the shed vortex moves away from the airfoil to a steady condition, a *bounded vortex* forms about the AC to counterbalance the shed vortex in accordance with *Kelvin's* circulation theorem [20]. The strength of the bound vortex is the algebraic sum of the shed vortices for all past time history. However, accurate tracking of all shed vortices is difficult especially when general airfoil motion is considered. A simple alternative is a harmonic motion assumption. So the application of the reduced frequency appropriately idealizes the vortex shedding as a function of the circular oscillation.

The flow around a harmonically oscillating airflow can be divided into two parts: the *circulatory* and *noncirculatory* effects [20]. The circulatory terms are

dependent on the vorticity of the flow field as mentioned above and tend to dominate the load calculation for oscillating airfoils. The noncirculatory terms develop instantaneously and are not dependent on the circulation. These terms result from the mass of air moving with the oscillating airfoil creating a reaction to the motion.

The harmonic assumption used in this study assumes developed pure harmonic motion where the transient effects of vortex initialization are neglected. This is a restricted, but applicable and classical technique for aeroelastic determination [30]. One significant drawback in using the harmonic assumption is that dependent aerodynamic theories can only predict the flutter speed and frequency or stability boundary. By definition, the harmonic time dependence of a system corresponds to the stability boundary where the system becomes critically damped [3]. Therefore, the modal damping and frequencies outside the flutter condition are estimated with techniques discussed in section 5.2.

5.1.3. Theodorsen's function

Theodorsen's function is used to model the changes in amplitude and phase of the unsteady forcing of harmonically oscillating airfoils [30]. The function is essentially a Fourier transform of the Wagner function, and it acts as a frequency domain filter for oscillating motion input to give a reduced frequency dependent output [5].

$$C(k) = F(k) + iG(k) = \frac{K_1(ik)}{K_0(ik) + K_1(ik)} \qquad 5.4$$

The function is a complex quantity with real $F(k)$ and imaginary $G(k)$ parts in order to model the phase and amplitude shifting. The $K_1(ik)$ and $K_0(ik)$ terms are modified Bessel functions of the second kind [20].

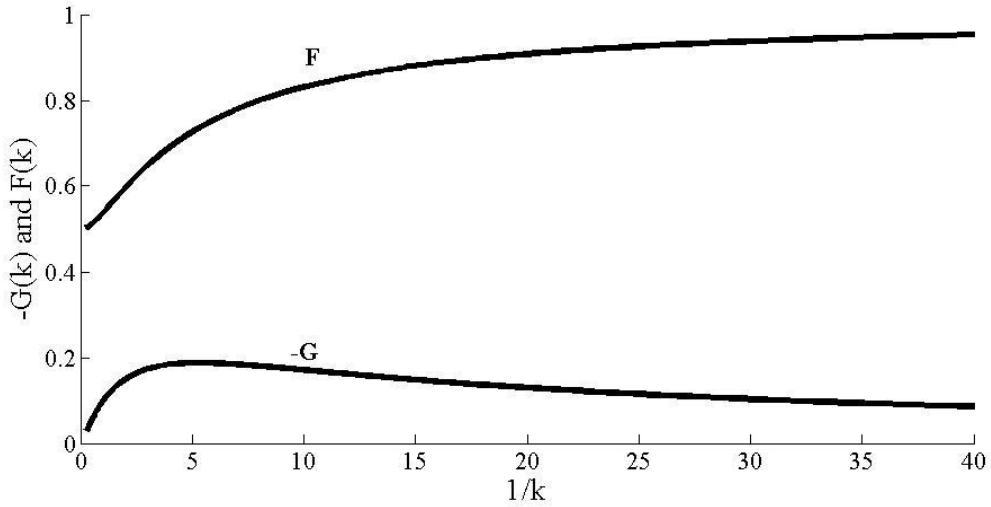

Figure 5.3 – Theodorsen's function for oscillating airfoil

The merit of Theodorsen's function is that it allows for accurate prediction of wake vortex shedding behavior for harmonically oscillating airfoils, which is critical to accurate unsteady lift calculation. Since the function is only applicable in the frequency domain, it a can only be used for stability analysis unless an inverse Fourier transform is applied to the function to convert it to the time domain. A representation of real and imaginary parts of Theodorsen's function is shown in Figure 5.3 as function of the reduced frequency [30]; this plot has comparable behavior to the Wagner function plot in Figure 5.1.

5.1.4. Unsteady aerodynamic derivatives

The linearized aerodynamic theory employed in this stability flutter analysis can be developed for an airfoil two-dimensional section to illustrate the application of unsteady effects. Considering the same symmetric airfoil section ($a_1 = 2\pi$) from Chapter 4 shown in Figure 4.1, the airfoil undergoes harmonic forcing and the linear response is of the form given in equation 3.1. The physical oscillatory response is then expressed for each coordinate respectively as

$$w = w_0 e^{i\omega t} \qquad \alpha = \alpha_0 e^{i\omega t}, \tag{5.5}$$

where the angle of attack is only a function of the elastic torsion as in equation 4.1. If the SC or FA is taken as the reference for physical displacement and the mid chord is taken as the geometric reference for the SC located a distance ab aft of the mid chord, the lift and moment equation per unit span are given[8, 20] as

$$\begin{aligned} L/\Delta y = {} & \pi\rho b^2[\ddot{w} + V\dot{\alpha} - ab\ddot{\alpha}] \\ & + 2\pi\rho bVC(k)\left[\dot{w} + V\alpha + b\left(\tfrac{1}{2} - a\right)\dot{\alpha}\right], \end{aligned} \tag{5.6}$$

$$\begin{aligned} M/\Delta y = {} & \pi\rho b^2\left[ab\ddot{w} - Vb\left(\tfrac{1}{2} - a\right)\dot{\alpha} - b^2\left(\tfrac{1}{8} + a^2\right)\ddot{\alpha}\right] \\ & + 2\pi\rho b^2 V\left(a + \tfrac{1}{2}\right)C(k)\left[\dot{w} + V\alpha + b\left(\tfrac{1}{2} - a\right)\dot{\alpha}\right]. \end{aligned} \tag{5.7}$$

These equations are derived by considering the noncirculatory and circulatory components of the flow field around the airfoil [5]. The noncirculatory terms listed first in each equation are dependent on the apparent moment of inertia or mass of the flow multiplied by the respective angular acceleration or vertical acceleration. The circular terms, which are dependent on Theodorsen's function,

account for the strength of the circulating vortex about the airfoil CP (¾ chord), and the response lag of the oscillating airfoil.

If the complex form of Theodorsen's function is applied along with a complex representation of the response displacement, equations 5.6 and 5.7 become

$$L/\Delta y = \{\pi\rho b^2[-\omega^2 w_0 + i\omega V\alpha_0 + \omega^2 ab\alpha_0] + 2\pi\rho bV(F+iG)\left[i\omega w_0 + V\alpha_0 + i\omega b\left(\tfrac{1}{2}-a\right)\alpha_0\right]\}e^{i\omega t}, \quad 5.8$$

$$M/\Delta y = \left\{\pi\rho b^2\left[-\omega^2 abw_0 - i\omega Vb\left(\tfrac{1}{2}-a\right)\alpha_0 + \omega^2 b^2\left(\tfrac{1}{8}+a^2\right)\alpha_0\right]\right\}e^{i\omega t} + \left\{2\pi\rho b^2 V\left(a+\tfrac{1}{2}\right)(F+iG)\left[i\omega w_0 + V\alpha_0 + i\omega b\left(\tfrac{1}{2}-a\right)\alpha_0\right]\right\}e^{i\omega t}. \quad 5.9$$

The equations can be linearized into the same form as the static lift equation used in Chapter 4,

$$L = qsc\frac{\partial C_L}{\partial \alpha}\alpha. \quad 5.10$$

However, the slope of the lift curve, $\frac{\partial C_L}{\partial \alpha}$, in the unsteady case is not just a function of the pitch incidence; rather it is function of non-dimensional displacement and velocity for plunge and pitch:

$$L_w = \frac{\partial C_L}{\partial\left({}^{w}/_{b}\right)}, \qquad L_{\dot{w}} = \frac{\partial C_L}{\partial\left({}^{\dot{w}}/_{V}\right)}, \qquad L_{\dot{\alpha}} = \frac{\partial C_L}{\partial\left({}^{\dot{\alpha}c}/_{V}\right)}, \quad \text{etc.} \quad 5.11$$

The resulting equations for lift and moment per unit span are written in terms of the *oscillatory aeroelastic derivatives* [30],

$$L/\Delta y = \rho V^2 b \left\{ (L_w + ikL_{\dot{w}}) \frac{w_0}{b} + (L_\alpha + ikL_{\dot{\alpha}})\alpha_0 \right\} e^{i\omega t} \qquad 5.12$$

$$M/\Delta y = \rho V^2 b^2 \left\{ (M_w + ikM_{\dot{w}}) \frac{w_0}{b} + (M_\alpha + ikM_{\dot{\alpha}})\alpha_0 \right\} e^{i\omega t} \qquad 5.13$$

which are given for the pitch and plunge DOF as shown in Table 5.1.

Table 5.1 – Oscillatory aeroelastic derivatives [5]

Derivatives	Unsteady – complex Theodorsen's values	Quasi-steady limit
$\boldsymbol{L_w}$	$= a_1 \left[-\frac{k^2}{2} - Gk \right]$	$= 0$
$\boldsymbol{L_{\dot{w}}}$	$= a_1 [F]$	$= a_1$
$\boldsymbol{L_\alpha}$	$= a_1 \left[\frac{k^2 a}{2} + F - Gk\left(\frac{1}{2} - a\right) \right]$	$= a_1$
$\boldsymbol{L_{\dot{\alpha}}}$	$= a_1 \left[\frac{1}{2} + F\left(\frac{1}{2} - a\right) - \frac{G}{k} \right]$	$= \infty^*$
$\boldsymbol{M_w}$	$= a_1 \left[-\frac{k^2 a}{2} + Gk\left(a + \frac{1}{2}\right) \right]$	$= 0$
$\boldsymbol{M_{\dot{w}}}$	$= a_1 \left[F\left(a + \frac{1}{2}\right) \right]$	$= a_1\left(a + \frac{1}{2}\right)$
$\boldsymbol{M_\alpha}$	$= a_1 \left[\frac{k^2}{2}\left(\frac{1}{8} + a^2\right) + F\left(a + \frac{1}{2}\right) - Gk\left(a + \frac{1}{2}\right)\left(\frac{1}{2} - a\right) \right]$	$= a_1\left(a + \frac{1}{2}\right)$
$\boldsymbol{M_{\dot{\alpha}}}$	$= a_1 \left[-\frac{k}{2}\left(\frac{1}{2} - a\right) + Fk\left(a + \frac{1}{2}\right)\left(\frac{1}{2} - a\right) + \frac{G}{k}\left(a + \frac{1}{2}\right) \right]$	$= \infty^*$

*Note: there is a singularity in the quasi-steady case as $k \to 0$ so the $\dot{\alpha}$ terms cannot appear in quasi-steady analysis

These aerodynamic loading terms can be rewritten in matrix form when the oscillatory response in equation 5.5 is substituted back into the loading giving [5]

$$\begin{Bmatrix} dL \\ dM \end{Bmatrix} = \left[\rho V \boldsymbol{B}^* \begin{Bmatrix} \dot{w} \\ \dot{\alpha} \end{Bmatrix} + \rho V^2 \boldsymbol{C}^* \begin{Bmatrix} w \\ \alpha \end{Bmatrix}\right] dy$$

$$\boldsymbol{B}^* = \begin{bmatrix} bL_{\dot{w}} & b^2 L_{\dot{\alpha}} \\ b^2 M_{\dot{w}} & b^3 M_{\dot{\alpha}} \end{bmatrix}, \quad \boldsymbol{C}^* = \begin{bmatrix} L_w & bL_\alpha \\ bM_w & b^2 M_\alpha \end{bmatrix}. \tag{5.14}$$

The $\boldsymbol{B}^*$ matrix is referred to as the *binary aerodynamic damping matrix* since its terms are proportional to the coordinate velocities. The $\boldsymbol{C}^*$ matrix is referred to as the *binary aerodynamic stiffness matrix* since its terms are proportional to the coordinate displacements. The 2x2 *binary* matrices only apply to the 2 DOF case typically investigated [5]. However, even in the in 2 DOF case, both matrices are nonsymmetric, which leads to the aeroelastic instability condition. The binary aeroelastic matrices $\boldsymbol{B}^*$ and $\boldsymbol{C}^*$ must be expanded for a FEM formulation to *n x n* size matrices, where *n* is the number of DOFs of the structural response element matrices. Thus, the structural response matrices and aerodynamic loading matrices are of the same order.

Applying strip theory aerodynamics, the lift and moment act on the elastic system as spanwise, generalized, unsteady forces where the incremental work energy formulation is in the form of the spanwise contribution in equation 3.7

$$\delta W_{ae} = \int_0^{s_{ae}} -dL\delta w + dM\delta\alpha. \tag{5.15}$$

The total load formulation of L and M in equations 5.12-5.14 is converted to the strip representation dL and dM when applying strip theory, by assuming distributed loading over an infinitesimal distance dy instead of a unit span as in equations 5.6-5.14:

$$dL = \rho V^2 \left[L_w w + L_{\dot{w}} \frac{b\dot{w}}{V} + L_\alpha b\alpha + L_{\dot{\alpha}} \frac{b^2\dot{\alpha}}{V} \right] dy \qquad \textbf{5.16}$$

$$dM = \rho V^2 b^2 \left[M_w bw + M_{\dot{w}} \frac{b^2\dot{w}}{V} + M_\alpha b^2\alpha + M_{\dot{\alpha}} \frac{b^2\dot{\alpha}}{V} \right] dy \qquad 5.17$$

In matrix form, the work done by the lifting load on a strip element is given as

$$W_{ae} = \int_0^{s_{ae}} \begin{Bmatrix} -w \\ \alpha \end{Bmatrix}^T \begin{Bmatrix} dL \\ dM \end{Bmatrix} \qquad 5.18$$

The plunge displacement w is negative because the bending displacement is positive nose down, which is opposite the convention for positive lift up.

The work energy can be written in terms of an assumed element interpolation function N in the form

$$W_{ae} = \int_0^{s_{ae}} \begin{Bmatrix} w_0 \\ \alpha_0 \end{Bmatrix}^T [N^e]^T \begin{Bmatrix} dL \\ dM \end{Bmatrix}. \qquad 5.19$$

The interpolation function N^e can be independent for each mode of interest:

$$N^e = \begin{bmatrix} -N_{bending} \\ N_{torsion} \end{bmatrix}. \qquad 5.20$$

Substituting the binary matrix formulation of equation 5.14 and the appropriate displacement interpolation gives

$$W_{ae} = \int_0^{s_{ae}} \begin{Bmatrix} w_0 \\ \alpha_0 \end{Bmatrix}^T \rho V \begin{bmatrix} -N_{bending} \\ N_{torsion} \end{bmatrix}^T \boldsymbol{B}^* \begin{bmatrix} N_{bending} \\ N_{torsion} \end{bmatrix} dy \begin{Bmatrix} \dot{w}_0 \\ \dot{\alpha}_0 \end{Bmatrix} + \int_0^{s_{ae}} \begin{Bmatrix} w_0 \\ \alpha_0 \end{Bmatrix}^T \rho V^2 \begin{bmatrix} -N_{bending} \\ N_{torsion} \end{bmatrix}^T \boldsymbol{C}^* \begin{bmatrix} N_{bending} \\ N_{torsion} \end{bmatrix} dy \begin{Bmatrix} w_0 \\ \alpha_0 \end{Bmatrix}. \quad 5.21$$

The full aerodynamic damping and stiffness matrices are then given as

$$\boldsymbol{B} = \rho V \int_0^{s_{ae}} \begin{bmatrix} N_{bending} \\ -N_{torsion} \end{bmatrix}^T \boldsymbol{B}^* \begin{bmatrix} N_{bending} \\ N_{torsion} \end{bmatrix} dy, \quad 5.22$$

$$\boldsymbol{C} = \rho V^2 \int_0^{s_{ae}} \begin{bmatrix} N_{bending} \\ -N_{torsion} \end{bmatrix}^T \boldsymbol{C}^* \begin{bmatrix} N_{bending} \\ N_{torsion} \end{bmatrix} dy. \quad 5.23$$

The sign of the aerodynamic matrices change once they are represented on the left hand side of the equations of motion instead of the right hand side for generalized forcing. The *n x n* aerodynamic matrix equations above, in conjunction with the structural *n x n* matrices, give the full ternary equations of motion, which are classically represented as a homogeneous stability problem [8, 20] in the form

$$\boldsymbol{A}\ddot{\varphi} + (\rho V \boldsymbol{B} + \boldsymbol{D})\dot{\varphi} + (\rho V^2 \boldsymbol{C} + \boldsymbol{E})\varphi = \boldsymbol{0}, \quad 5.24$$

where $\boldsymbol{A}, \boldsymbol{D}, \boldsymbol{E}$ are the structural inertia, structural damping, and structural stiffness respectively, and φ are the generalized coordinates. The $\boldsymbol{B}$ and $\boldsymbol{C}$ matrices only apply for a specific reduced frequency of interest unlike the structural equations which are typically constant for all linear considerations. Thus, a frequency

matching or balancing method is necessary to determine the displacement dependent aerodynamic components that in turn determine the displacement stability characteristics of the ternary system. Since the equation of motion is homogeneous with a zero right hand side, it is not possible to determine the absolute values of the modal response. Instead, an eigensolution approach is necessary.

5.2. Eigenvalue and Frequency Matching Solution Methods

In order to properly model aeroelastic systems, unsteady, reduced frequency dependent aerodynamics must be included in the analysis. The characteristic determinate eigensolution of equation 5.24 can be solved directly when the $\boldsymbol{B}$ and $\boldsymbol{C}$ matrices are known. However, the matrices cannot be formed until the reduced frequency is known, and the reduced frequency is dependent on the eigensolution. Thus, there is no direct method to solve the equations of motion and an iterative *frequency matching* is typically used.

The two techniques described in this section rely on the harmonic response assumption, which can predict the stability boundary but not the subcritical behavior. Thus the methods should accurately predict the flutter speed and frequency, but will inherently predict different subcritical behavior. However, the stability boundary information is sufficient to show the mechanism of flutter in the form of negative modal damping, which allows the engineer to make design variations to prevent the stability altogether. The "baseline system" used in this

section to illustrate and verify the frequency matching techniques is given by Wright [5] for an elastic spring, binary, airfoil with simplified unsteady flow approximations. The baseline data is not printed here because it does not apply to the FEM formulation.

5.2.1. The 'k' method

A practical observation of a harmonically oscillating airfoil shows that the total energy removed per cycle or the total damping is a function of the square of the amplitude and is independent of the frequency of oscillation [3]. Thus, a complex stiffness or hysteretic damping as mentioned in section 3.2.2.2 is characteristic of the system. If the structural damping is incorporated in the formation of the equations of motion as a function of the unknown structural damping coefficient, g,

$$\boldsymbol{D} = ig\boldsymbol{E} \tag{5.25}$$

then harmonic equation of motion is of the form [5]

$$\left[\boldsymbol{A} + i\rho\left(\frac{b}{k}\right)\boldsymbol{B} - \rho\left(\frac{b}{k}\right)^2\boldsymbol{C} + \frac{1+ig}{\omega^2}\boldsymbol{E}\right]\varphi_0 = \boldsymbol{0}. \tag{5.26}$$

This equation is a generalized eigenvalue problem,

$$\begin{gathered}\left(\boldsymbol{F} - \tilde{\lambda}\boldsymbol{E}\right)\varphi_0 = 0 \\ \text{where } \boldsymbol{F} = \left[\boldsymbol{A} + i\rho\left(\tfrac{b}{k}\right)\boldsymbol{B} - \rho\left(\tfrac{b}{k}\right)^2\boldsymbol{C}\right], \text{ and} \\ \tilde{\lambda}_j = \frac{1+ig_j}{\omega_j^2}.\end{gathered} \tag{5.27}$$

The coupled oscillating frequency and structural damping of each respective DOF is based on the corresponding complex eigenvalue

$$\omega_j = \frac{1}{\sqrt{Re(\tilde{\lambda}_j)}}, \qquad g = 2\zeta = \frac{Im(\tilde{\lambda}_j)}{Re(\tilde{\lambda}_j)}. \tag{5.28}$$

The ζ term is the equivalent damping ratio at the natural frequency. The *k* method is implemented in a step-by-step process outlined below [5]:

1. Choose a reduced frequency (k) of interest, usually near zero.
2. Calculate the corresponding aerodynamic stiffness $\boldsymbol{B}$ and damping $\boldsymbol{C}$ matricies.
3. Solve the Eigen problem of equation 5.27 for the complex eigenvalues.
4. Determine the corresponding frequency and damping from equation 5.28.
5. Relate the oscillating frequency and the selected reduced frequency from step 1 to the forward velocity based on the definition of the reduced frequency from equation 5.3.
6. Repeat steps 1-5 until the range of *k* values has been investigated.
7. Assemble the calculated values of frequency with respect to velocity for each respective mode by ploting the calucated frequnecy with respect to its corresponding velocity in a "shooting method" from the FD origin. An example assembly is shown in Figure 5.4 for 3 separate reduced frequencies and 2 modes of interst

A 2 DOF sample for three values of reduced frequency is shown in Figure 5.4, which is a plot of the modal frequencies over the velocities of interest known as $V\omega$ plot. For each reduced frequency *k*, there are two complex eigenvalues corresponding to each modal frequency and damping value. The trend of the system and the mechanism of flutter can then be predicted with a *Vg* plot, which relates the modal damping ratio *g* from equation 5.28 as a function of the respective velocity. However, the equivalent damping ratio ζ is used instead to maintain consistency with the 'p-k' formulation. An example *Vg* plot is shown in Figure 5.5 for the same

two modes of interest as in Figure 5.4. The damping ratios of each mode of interest start at zero percent critical when the wind is off and the flow velocity is zero. As the flow velocity increases the reduced frequency definition in equation 5.3 requires that the modal oscillation frequency compensate for a constant reduced frequency. Thus, the individual modal frequencies tend to coalesce to a common flutter frequency as the velocity increases.

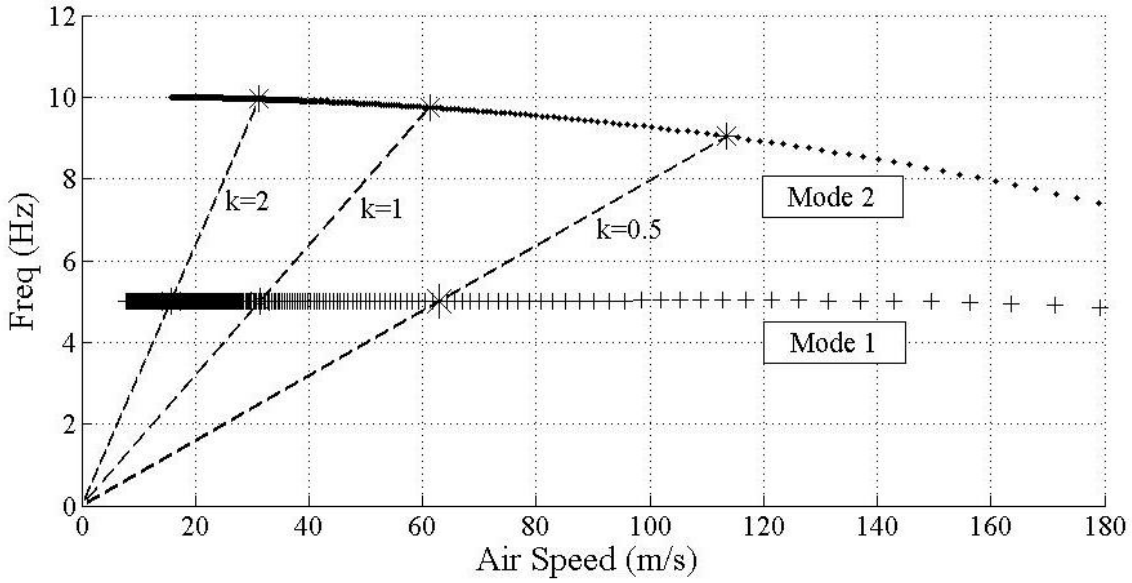

Figure 5.4 – Example 'k' method *Vω* frequnecy plot of the basline system for lines of constant reduced frequency ------ and 2 modes of interest

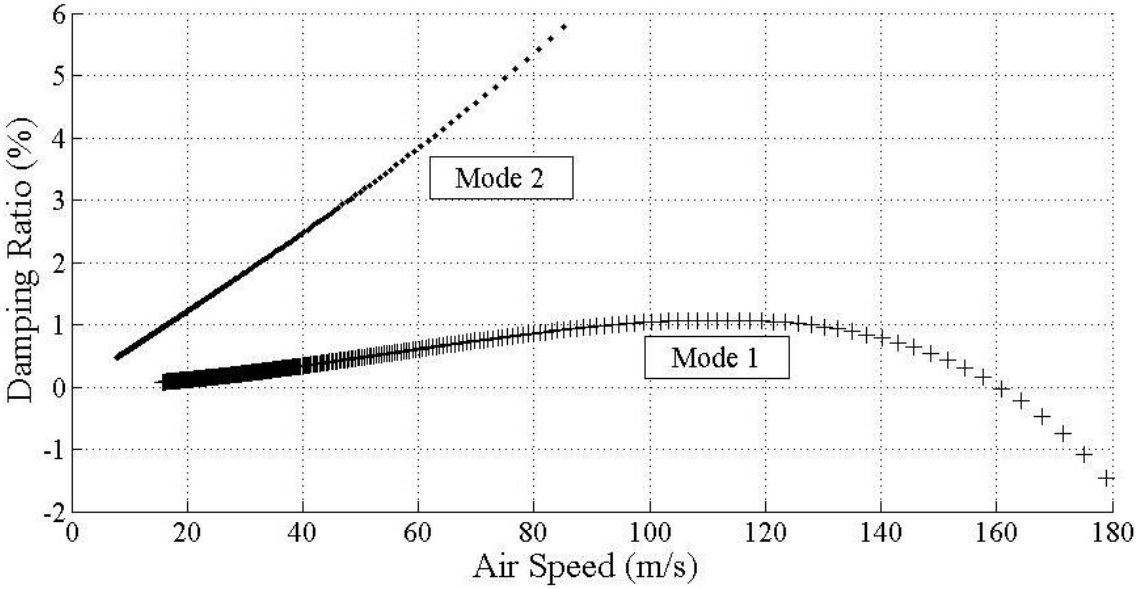

Figure 5.5 – Example 'k' method *Vg* plot with 2 modes of interest

Assuming the convention that work into a system is negative; the aeroelastic system draws energy from the airstream as the phasing of the torsion and bending coalesce shown in Figure 5.6. The energy input into the system causes the structure to oscillate at the coalescence frequency, thus simultaneously exciting both modes resulting in flutter. So the flutter velocity V_F is the point when the damping of a single mode crosses the zero damping line from positive modal damping to negative modal damping. In Figure 5.5, $V_F = 161\ m/s$ where the damping is critical. The corresponding dimensionless reduced frequency is $k = 0.31$ giving a flutter frequency of $\omega_F = 7.9$ Hz with a unit semi-span.

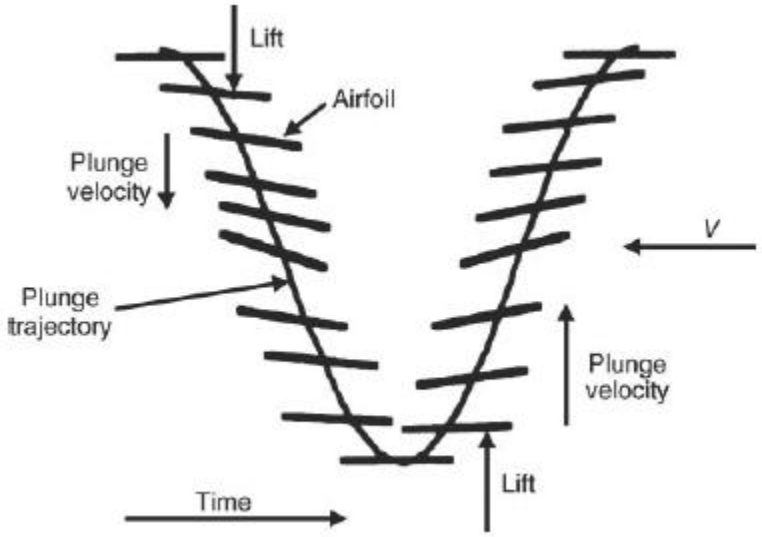

Figure 5.6 – Pitch and plung phasing shown near the same frequency to produce coalescence and instability [10]

The addition of the hysteretic damping in the 'k' method eigensolution is artificial in that the total damping is designed to give a zero value at the critical condition [7]. So the non-critical behavior is suspect and can lead to incorrect damping trends. A more direct iteration scheme called the 'p-k' method relies on an experimental determination of the strucutral damping, and iterates directly over a span of velocities instead of shooting from the origin when iterating over a span of reduced frequencies.

5.2.2. The 'p-k' method

The *k* method is a convenient formulation for prediction of the critical flutter speed, but it is a mathematically improper formulation since it imposes artificial structural damping. A proportional damping *p-k* method demonstrated by Hassig

[33] better approximates the true damping solution of lightly damped lower modes by incorporating proportional damping, and it compares accurately to general transient loading at small deflections. The aeroelastic equation 5.24 must first be reduced to a first order form by considering the trivial equation

$$\boldsymbol{I}\dot{\varphi} - \boldsymbol{I}\dot{\varphi} = 0, \tag{5.29}$$

where $\boldsymbol{I}$ is the identity matrix. Combined with equation 5.24 in partitioned or state-space form gives the formulation

$$\begin{bmatrix} \boldsymbol{I} & 0 \\ 0 & \boldsymbol{A} \end{bmatrix} \begin{Bmatrix} \dot{\varphi} \\ \ddot{\varphi} \end{Bmatrix} - \begin{bmatrix} 0 & \boldsymbol{I} \\ -(\rho V^2 \boldsymbol{C} + \boldsymbol{E}) & -(\rho V \boldsymbol{B} + \boldsymbol{D}) \end{bmatrix} \begin{Bmatrix} \varphi \\ \dot{\varphi} \end{Bmatrix} = \begin{Bmatrix} 0 \\ 0 \end{Bmatrix}. \tag{5.30}$$

Or the equation can be rewritten in first order form for a classical eigensolution

$$\begin{Bmatrix} \dot{\varphi} \\ \ddot{\varphi} \end{Bmatrix} - \begin{bmatrix} 0 & \boldsymbol{I} \\ -\boldsymbol{A}^{-1}(\rho V^2 \boldsymbol{C} + \boldsymbol{E}) & -\boldsymbol{A}^{-1}(\rho V \boldsymbol{B} + \boldsymbol{D}) \end{bmatrix} \begin{Bmatrix} \varphi \\ \dot{\varphi} \end{Bmatrix} = \begin{Bmatrix} 0 \\ 0 \end{Bmatrix}. \tag{5.31}$$

Assuming harmonic motion, the eigensolution is in the form

$$(\boldsymbol{Q} - \tilde{\lambda}_j \boldsymbol{I})\tilde{\phi}_j = 0 \tag{5.32}$$

The eigenvalues of the system matrix $\boldsymbol{Q}$ are complex conjugate pairs, and the oscillatory frequency and damping are functions of the real and imaginary components [58],

$$\tilde{\lambda}_j = \zeta_j \omega_j \pm i\omega_j \sqrt{1 - \zeta_j^2}, \qquad j = 1, 2, \dots, N. \tag{5.33}$$

The corresponding eigenvectors appear in complex conjugate columns where the upper half of the eigenvectors correspond to the complex mode shapes

$$\tilde{\phi}_j = \begin{Bmatrix} \varphi_j \\ \lambda\varphi_j \end{Bmatrix}, \quad j = 1, 2, \ldots, N.$$

The resulting modal frequencies and damping can be calculated from the complex eigenvalues with the functions

$$\omega_j = \sqrt{\left(Re(\tilde{\lambda}_j)\right)^2 + \left(Im(\tilde{\lambda}_j)\right)^2}, \qquad \zeta = \frac{Re(\tilde{\lambda}_j)}{\omega_j}. \tag{5.34}$$

The *p-k* method is implemented in an iterative manner described below [5]:

1. Select an airspeed of interest.
2. Select a mode of interest from among the degrees of freedom.
3. Guess the initial oscillation frequency for the mode using the wind off natural frequency or the previous airspeed.
4. Calculate the reduced frequency for this condition from equation 5.3.
5. Calculate the corresponding aerodynamic stiffness $\boldsymbol{B}$ and damping $\boldsymbol{C}$ matricies.
6. Solve the Eigen problem of equation 5.31 for the complex eigenvalues.
7. Calculate the oscillatory frequencies of the system using the eigenvalue of the real $\boldsymbol{Q}$ matrix.
8. Take the system frequency closest to the initial guess step 3 and repeat steps 4-7.
9. Continue iterating until the difference between the initial guess and the final frequency is less than some tolerance value near zero.
10. Consider the next mode of interest and repeat steps 3-9 until all modes of interest for the flight condition are investigated.
11. Consider the next airspeed of interest and repeat steps 2-10 until all flight speeds of interest are investigated.
12. Assemble the frequency and damping, which now applies directly to each mode.

The *Vω* and *Vg* plots can be drawn as before, except that the modal frequencies and damping ratios are stored directly for each velocity in the span of interest. The accuracy of the *p-k* method depends on the damping associated with each particular mode. The proportional viscous structural damping described in

section 3.2.2.1 is applied at the system level with Rayleigh coefficients and not at the modal level so only the damping on the lowest modes should be considered. The aerodynamic damping term is modally dependent, and usually dominates the total damping at higher airspeeds, so the *p-k* method does predict accurate behavior for lower lightly damped modes [3].

A comparison of the *p-k* and *k* flutter solution methods in Figure 5.7 shows that both methods predict the flutter boundary at exactly the same fluid velocity. The damping of the lower bending mode becomes negative at 161 m/s as the torsion frequency approaches the bending frequency, exactly as in the 'k' method solution. However, the structural damping is not a necessary component of the 'p-k' solution so the effect of variable structural damping can be investigated. The modal data is nearly identical to the 'k' method solution except that the damping trend of the lower mode is under predicted by the 'k' method.

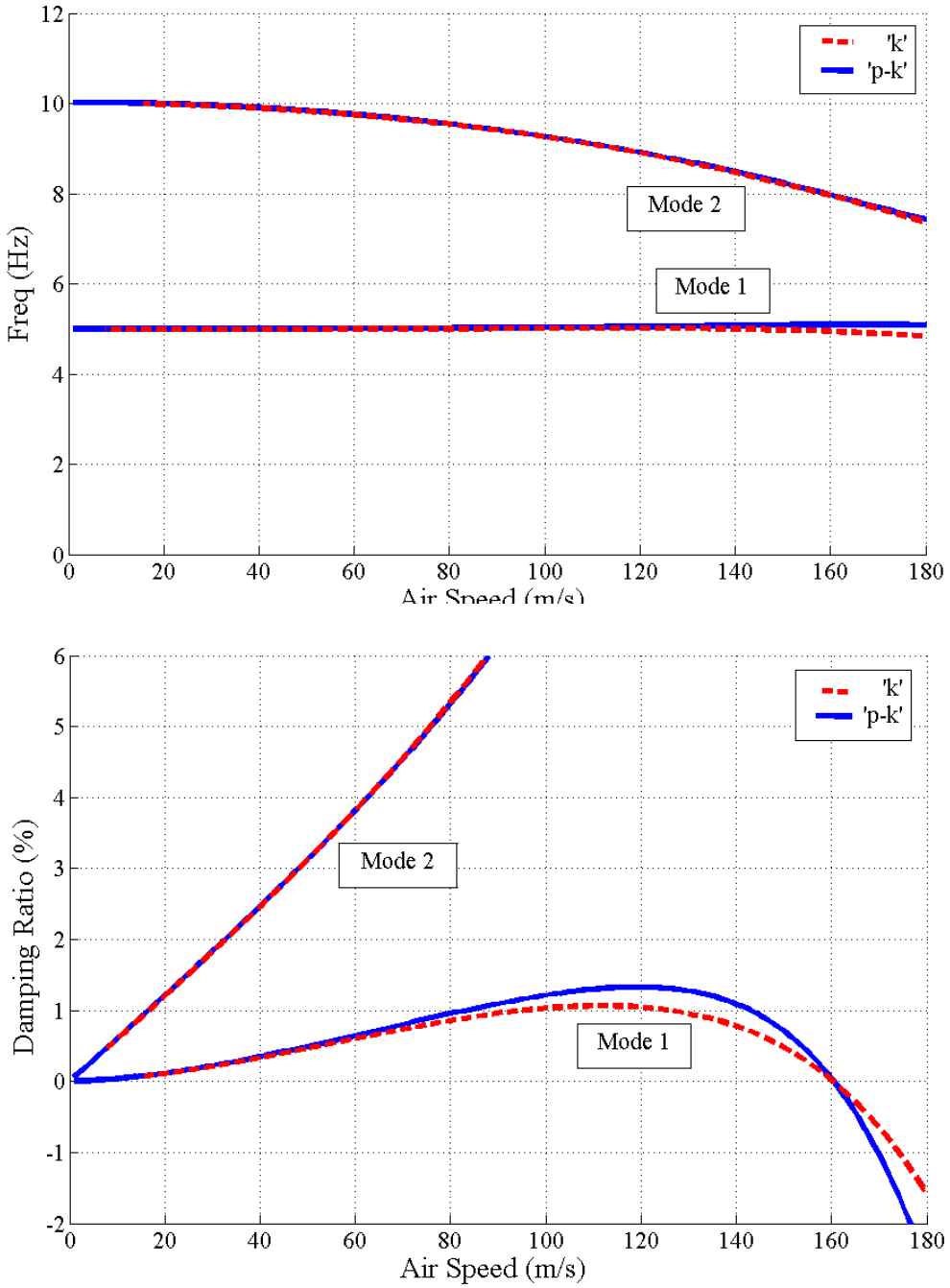

Figure 5.7 – Sample comparison Vω and Vg plots for flutter solution methods: ------ 'k' and —— 'p-k'

5.3. Validation

The 'p-k' flutter model was used in all subsequent flutter calculations, and is validated here by the classical Goland square wing, which has readily available exact flutter characteristics [39]. The square cantilever wing material data is listed in Table 3.1 with additional characteristics and International Standard Atmosphere (ISA) flow properties listed in Table 5.2.

Table 5.2 – Case study geometry and flow properties

Wing		**Flight Condition**	
Center of Gravity Shear Center	43% chord 33% chord	Altitude Speed of Sound ρ_{air}	9.14 [km] 303.1 [m/s] 0.46 [kg/m^3]

The $V\omega - Vg$ plots of the data are shown in Figure 5.8 for incompressible flow using one cubic interpolation element for bending, torsion and loading. The wing flutters at approximately $V_f = 170.3\ m/s$ $(Ma = 0.56)$ where the damping of the second mode becomes negative as indicated by the vertical line. The flutter velocity is essentially exact as compared to reference [39]. The flutter frequency $(\omega_F = 13.1\ Hz)$ is determined from a root locus style plot of the frequency over the negative damping ratio shown in Figure 5.9. Both plot types are necessary for an understanding of the system behavior in the frequency domain.

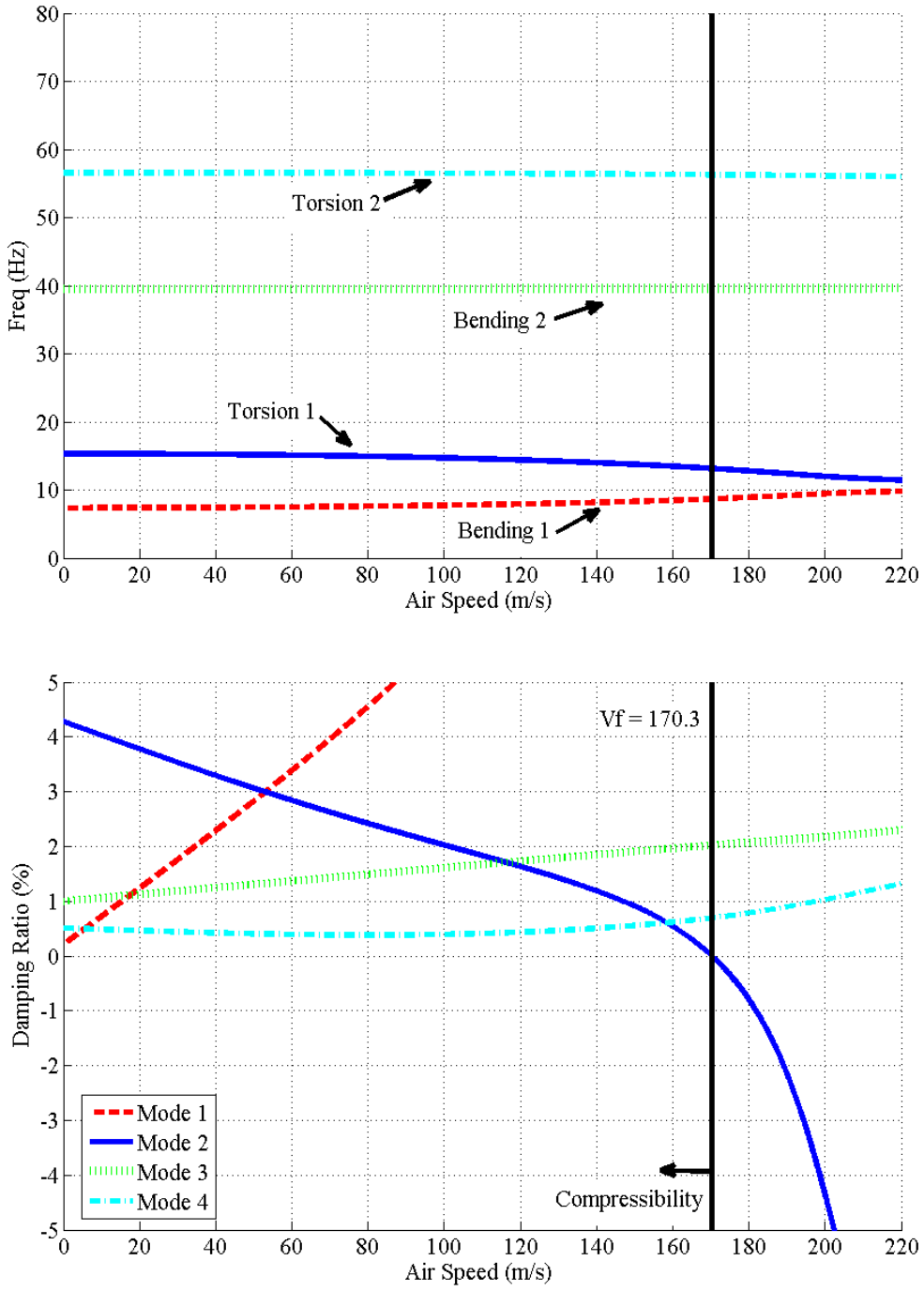

Figure 5.8 – Vω and Vg plots of Goland square cantilever wing with consistent cubic interpolation

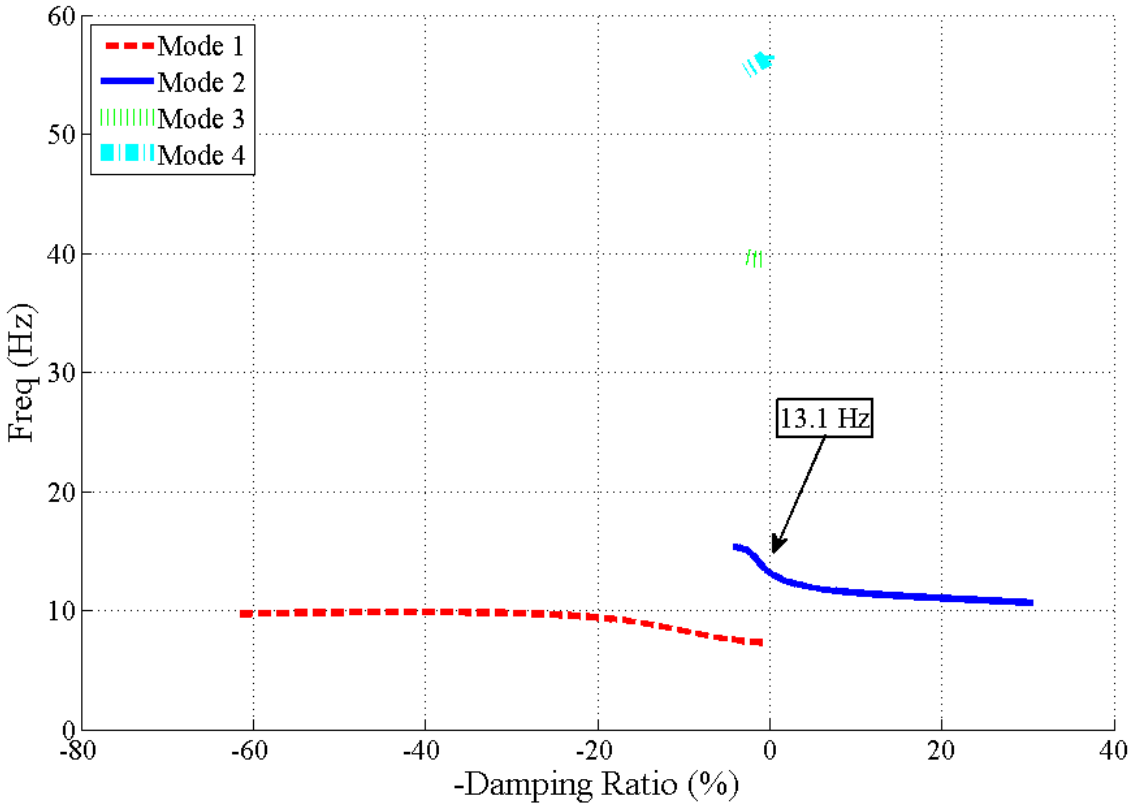

Figure 5.9 – Frequency vs. damping ratio root locus for Goland wing configuration with cubic interpolation

Both the $V\omega - Vg$ plots and the root locus plots describe the stability of the system. The $V\omega - Vg$ plots show the distribution of the modal damping over the flight velocity regime and the upper bound of the regime is determined by transonic effects at roughly 220 m/s ($Ma \approx 0.7$) . The Goland lifting model does not account for compressibility effects as mentioned in section 4.2.1, so the plots above necessarily overestimate the flutter behavior beyond $Ma \approx 0.3$. However, the compressibility does not dramatically affect the trend of the modal behavior, and the flutter speed with compressibility is shown in Figure 5.8 at 158 m/s.

Compressibility only affects the fluttering mode and as a result, the fluttering second mode interacts with the first mode at a lower velocity.

The root locus plot in Figure 5.9 shows the modal distribution of the damping at the characteristic system oscillations. The real axis of the root locus plot is represented by the damping ratio and when the second mode crosses the critical zero real value, the system becomes unstable as shown by the location of the flutter frequency. The two lower modes of bending and pitch are the most sensitive to characteristic oscillations as shown by the expression of a range of damping for those modes. The higher modes need not be considered in this case since they are not manifest as a range of damping for the higher frequencies. Additionally, real aircraft systems experience oscillations in the range of 0-60 Hz as mentioned in section 2.2, so any oscillations near or above this range can be neglected, such as the fourth characteristic mode in this case.

The design of the strucutral system determines the resulting aeroelastic behavior. The parametric plot shown in Figure 5.10 is an example of the flutter speed dependence on the mass axis (MA) and flexural (FA) locations. The Goland square wing appears on the surface, near the minium of the flutter speed plot, which means that the strucutral design is very conservative. The flutter speed can be increased by moving the MA (x_{CG}) forward or moving the FA (x_{SC}) aft. The bisecting line in the middle of the plot shows the MA and FA as coincident, which demonstrates the effect of the distance *ec* to the aerodyanmic axis (AA). As the

coincident MA and FA move forward, the flutter speed increases since the moment arm *ec* of the unsteady loading acting about the AA decreases.

The bounds of the parametic plot in Figure 5.10 are set by the inherent strucutral system stability. If the distantce between the MA and FA, e_m is greater than roughly 20% of the chord length the structral system becomes indeterminate due to positive and negative distribution of the eigenvalues indpendent of the aerodynamic forcing. If the structural system is marginally unstable, then the wind-off natural frequencies are not real values, and the aeroelastic system becomes complex. If the aeroelastic matrix is complex, then the 'p-k' method breaks down, and flutter determination is not possible.

The unsteady aerodyanmic contribution is consistently modeled with Theodorsen's functions and essentially determines the flutter speed. However, the flutter speed estimation is suspect at values in the transonic region due to thermal effects, so the flat areas in the farfield of the plot are a representation of the lack of confidence in the the flutter estimation at those configurations. The calculations below the flat area are reasonable and expected (see [5] pp 180). All aeroelastic configurations in Figure 5.10 are longitudinally, statically stable [54] meaning that static aerodyanmic effetcs would not cause divergence even if rigid body motion is considered. This is important since static divergence, as mentioned in section 4.3, is apparent for long slender wings covered in following numerical examples.

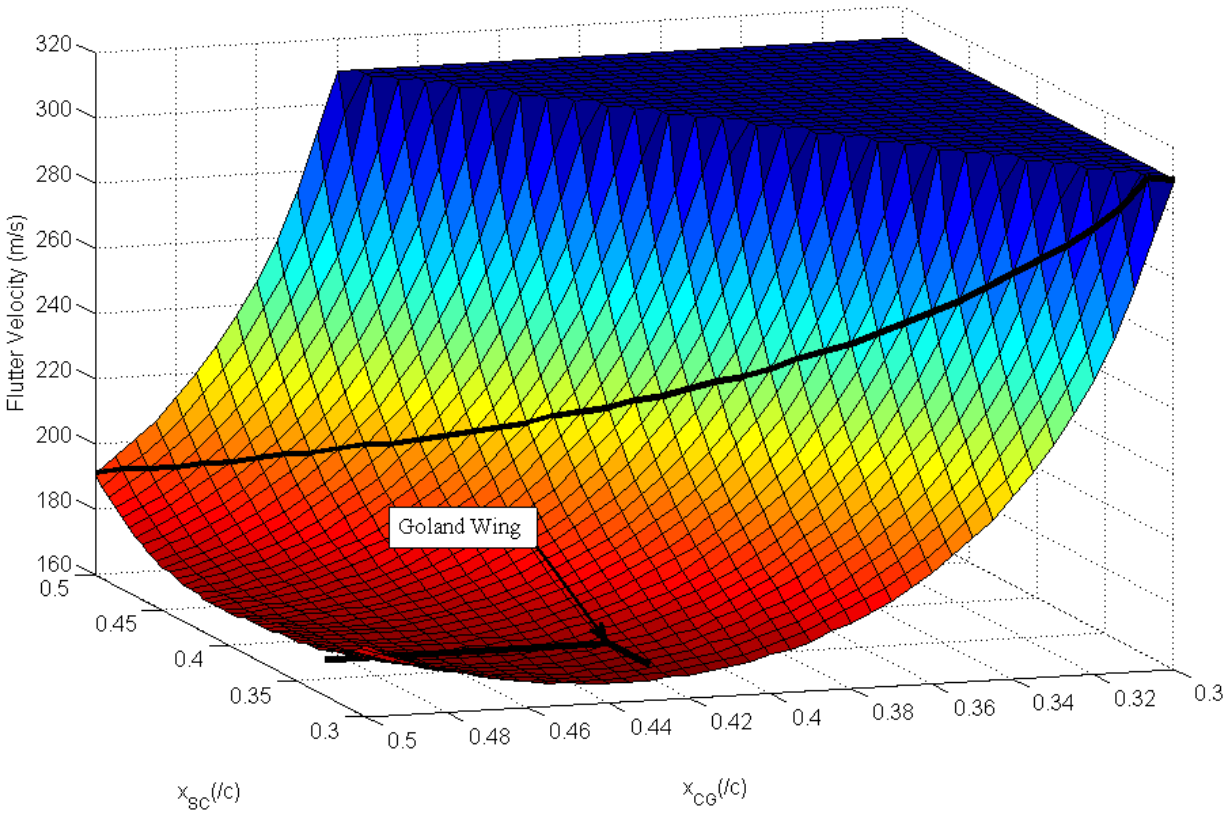

Figure 5.10 – Parametric study of the flutter velocity dependence on the wing flexural axis and mass axis location

Chapter 6

Computational Flutter Analysis

The FEM can be effectively applied to aeroelastic flutter because of its versatility. The effects of aerodynamic damping and stiffness, complex lifting surface configuration [59], and anisotropic material properties [60] can be conveniently included. This chapter will focus on the formulation of the FEM for application to idealized lifting surfaces. A comparison of the linear flutter boundary results to analytical solutions demonstrates excellent accuracy of the proposed formulation.

6.1. Computational Flutter Model

The implementation of the FEM based flutter analysis is developed entirely within a simple MATLAB program without relying on external commercial FEM, or aerodynamic codes. The assembly of the structural element matrices follows the usual manner and will not be discussed. However, the structural system is used to

determine the wind off characteristic eigenvalues and respective natural frequencies with the MATLAB function *eig* [61]. The function relies on Cholesky factorization for the symmetric structural system and produces only real eigenvalues. The natural frequencies are then used in a 'p-k' style algorithm to determine the distinct flutter speed. The MATLAB function *besselk* [62] was used to determine the components of Theodorsen's function for the calculation of unsteady strip aerodynamics. Finally, the MATLAB function *eig* is used to determine the nonsymmetric aeroelastic characteristic in equation 5.30-5.32. The function relies on QZ factorization for the nonsymmetric aeroelastic first order matrix, and produces complex eigenvalues and eigenvectors [63]. The algorithm is presented in Figure 6.1 based on the method described in section 5.2.2.

6.2. Numerical Examples

The application of this linear flutter model to real world examples is an important and necessary validation of the techniques considered herein. High-Altitude Long Endurance (HALE) aircraft are a unique example for comparison due to extremely large aspect ratio wings ($AR > 10$). The long slender wings of HALE aircraft are prone to large deflections as a result of an interaction with the airflow, but at cruise conditions with minimal deflection the linear analysis accurately predicts the flutter stability [18]. Table 6.1 gives the case study data for the HALE aircraft of interest, which are taken from reference [64].

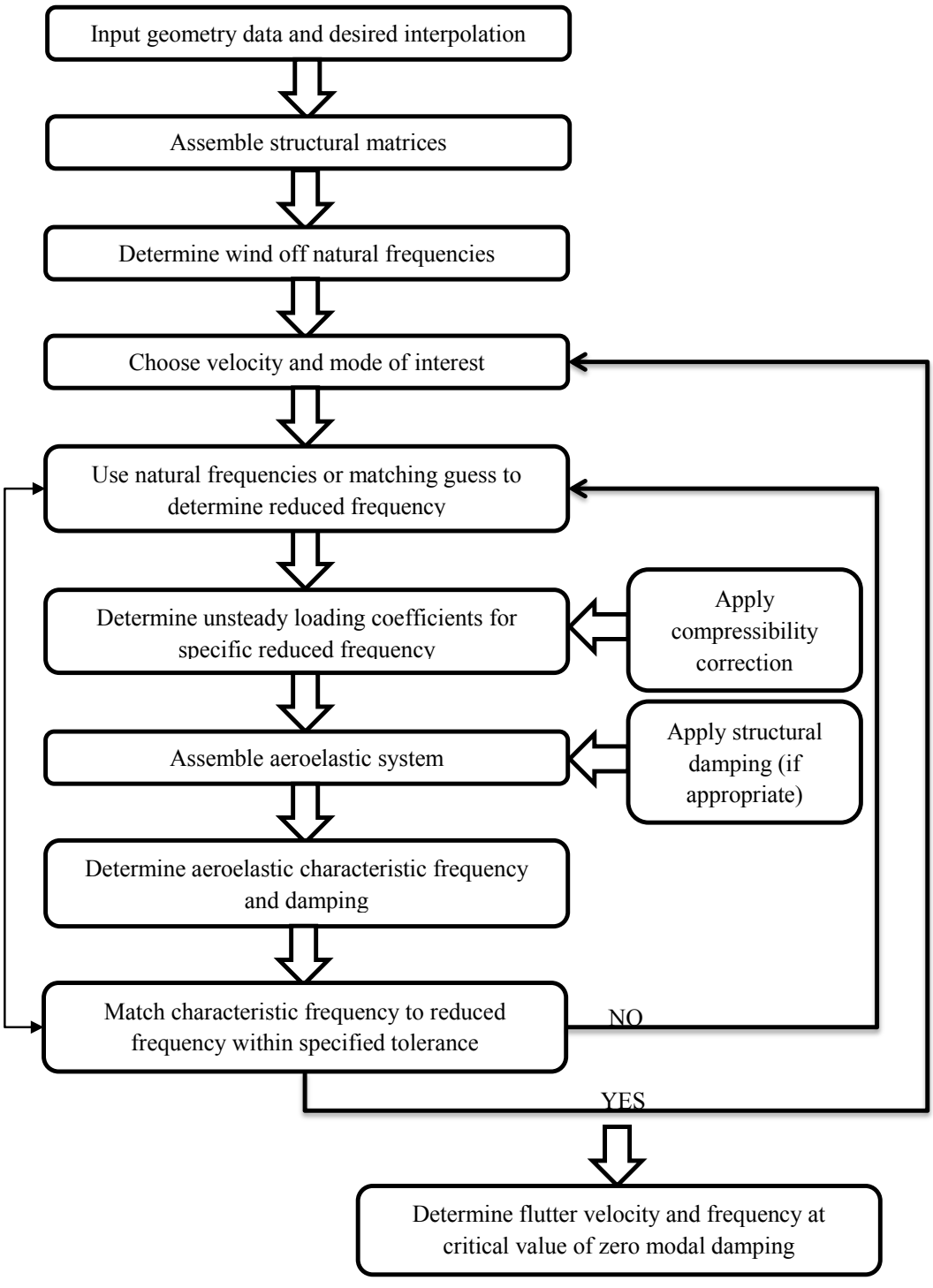

Figure 6.1 – Linear flutter 'p-k' algorithm

Table 6.1 – HALE aircraft case study data

Wing		**Flight Condition**	
Half span	16 [m]	Altitude	20 [km]
Chord	1 [m]	Speed of Sound	295.1 [m/s]
Mass density	0.75 [kg/m]	ρ_{air}	0.088 [kg/m^3]
Polar moment area	0.033 [m^4]		
Center of Gravity	50% chord		
Shear Center	50% chord		
Bending Rigidity	2 x 10^4 [Nm^2]		
Torsional Rigidity	1 x 10^4 [Nm^2]		

The linear flutter speed and frequency are calculated as 33.1 m/s and 21.4 rad/s respectively. A comparison to the published results is shown in Table 6.2 for multiple cases. The calculated linear cases demonstrate excellent agreement with the published results. The published values are determined with 8 finite elements in a similar manner to the technique presented herein, except that a finite-state aerodynamic model is used instead to represent the aero loads in a set of time-domain differential equations [3]. The calculated results are shown for various numbers of elements and interpolations, but the flutter speed results converge monotonically with the addition of more elements. The various $V\omega - Vg$ plots for each calculated case are shown in Figure 6.2 through Figure 6.4.

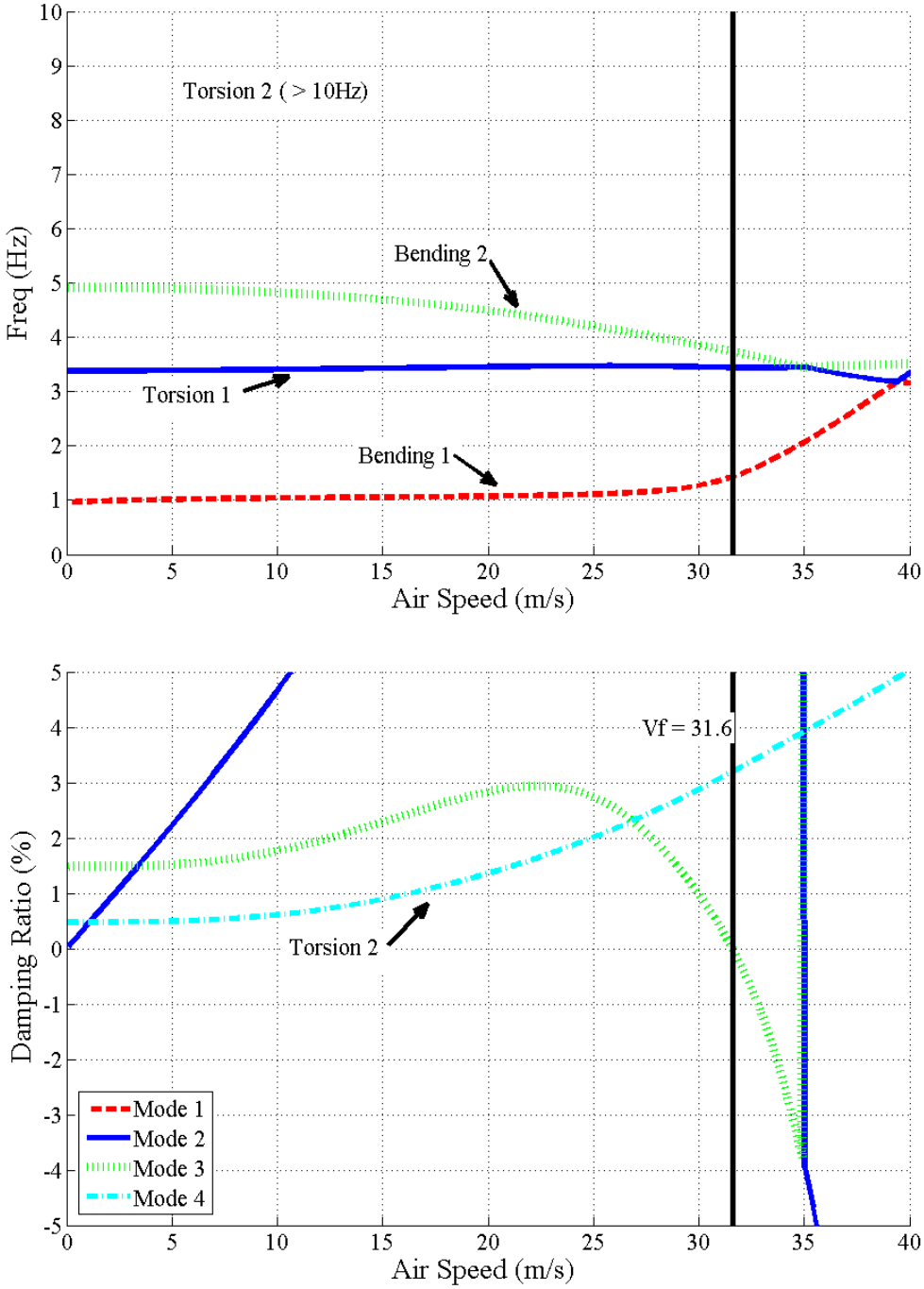

Figure 6.2 – Vω and Vg plots with 1 element cubic interpolation

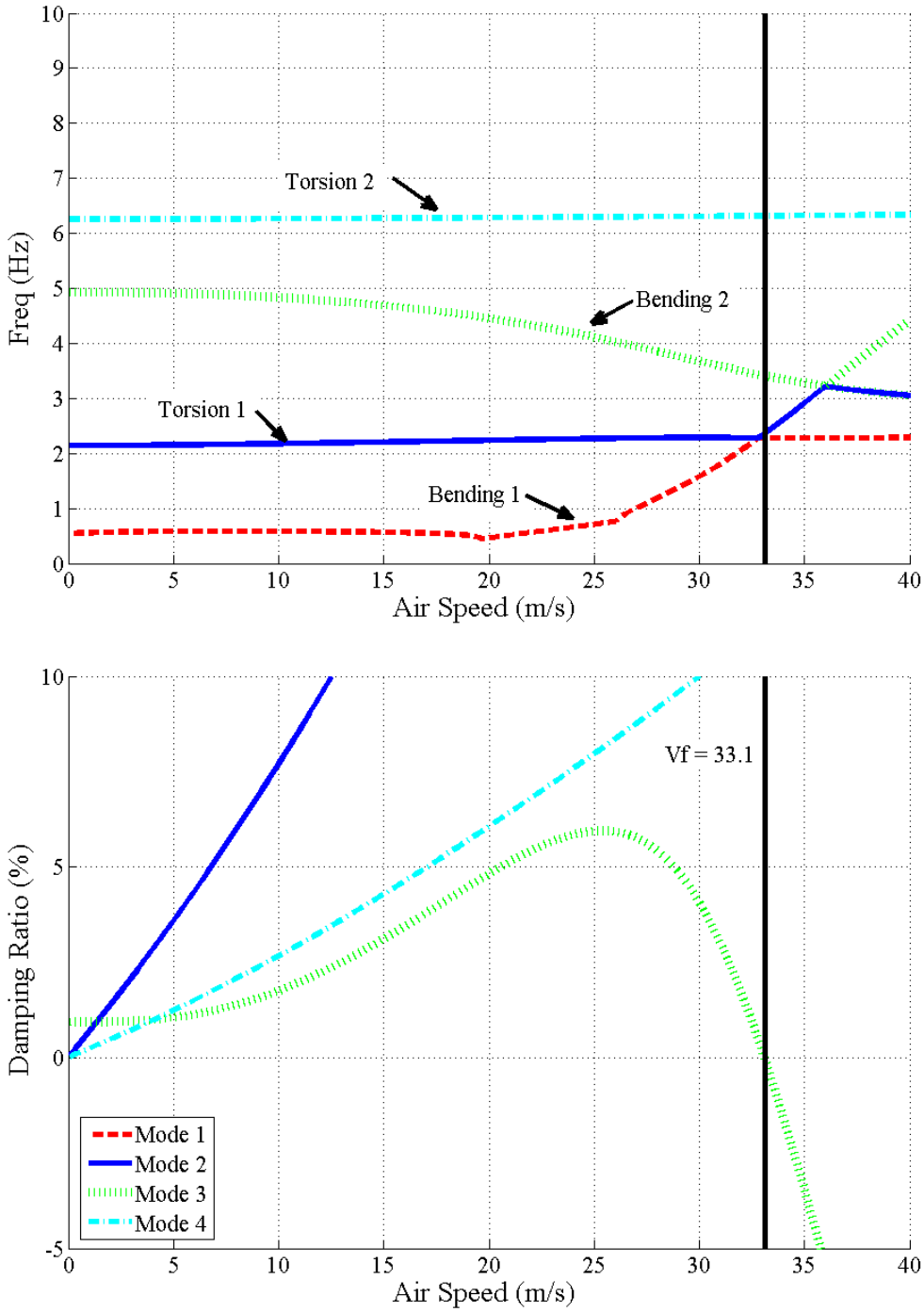

Figure 6.3 – Vω and Vg plots with 5 element cubic interpolation

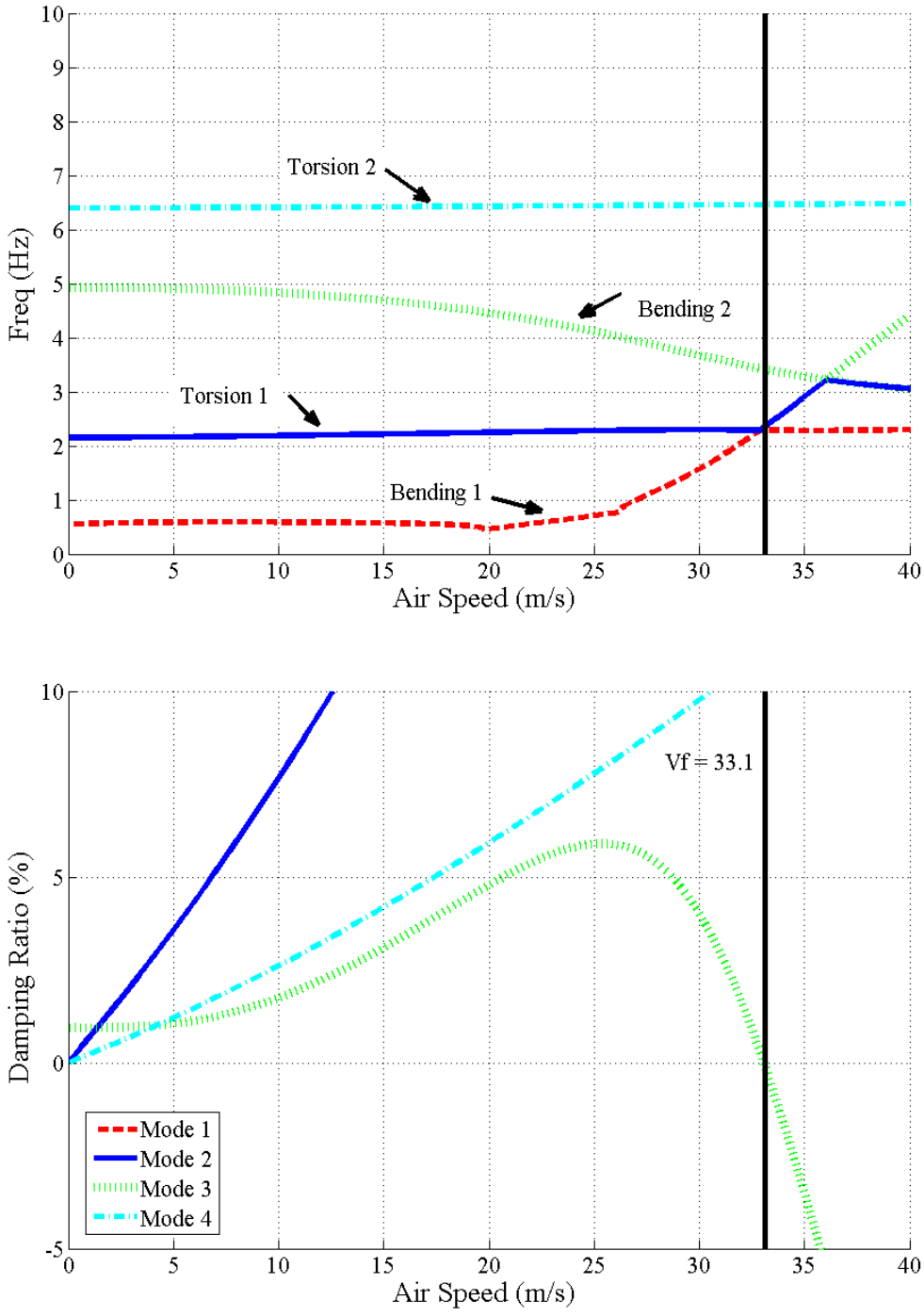

Figure 6.4 – Vω and Vg plots with 1 element quintic interpolation

Table 6.2 – Comparison of linear flutter results

	Flutter Speed [m/s]	Flutter Frequency [Hz]
8-e Analysis of [64]	32.2	3.40
1-e cubic interpolation	31.6	3.73
5-e cubic interpolation	33.1	3.41
1-e quintic interpolation	33.1	3.41

The cubic interpolation effectively predicts the low order or "binary" effects of the first two modes of bending and torsion, but is a poor predictor of the higher order effects. The cubic interpolation under predicts the behavior of the second bending (Mode 3) and second torsion (Mode 4) modes, leading to an overly conservative estimation of the flutter velocity as shown in Figure 6.2. The modal behavior is accurately captured with 5 cubic elements as shown in Figure 6.3. The coalescence of the first two modes combined with the high damping of the lowest bending mode (Mode 1) results in a manifestation of flutter behavior in Mode 3 as it extracts energy from the coalescence of all three lower modes. The fourth mode does not interact with the lower modes, but the damping trend is not well predicted by low order cubic interpolation.

The quintic interpolation accurately predicts the lower and higher order modes of interest especially in high aspect ratio wings. The plot in Figure 6.4 shows excellent agreement with the converged flutter solution, with only one element. The higher mode effects cannot be neglected in this case as shown by Figure 6.5,

therefore, the quintic interpolation is well suited for low DOF linear analysis of high aspect ratio wings.

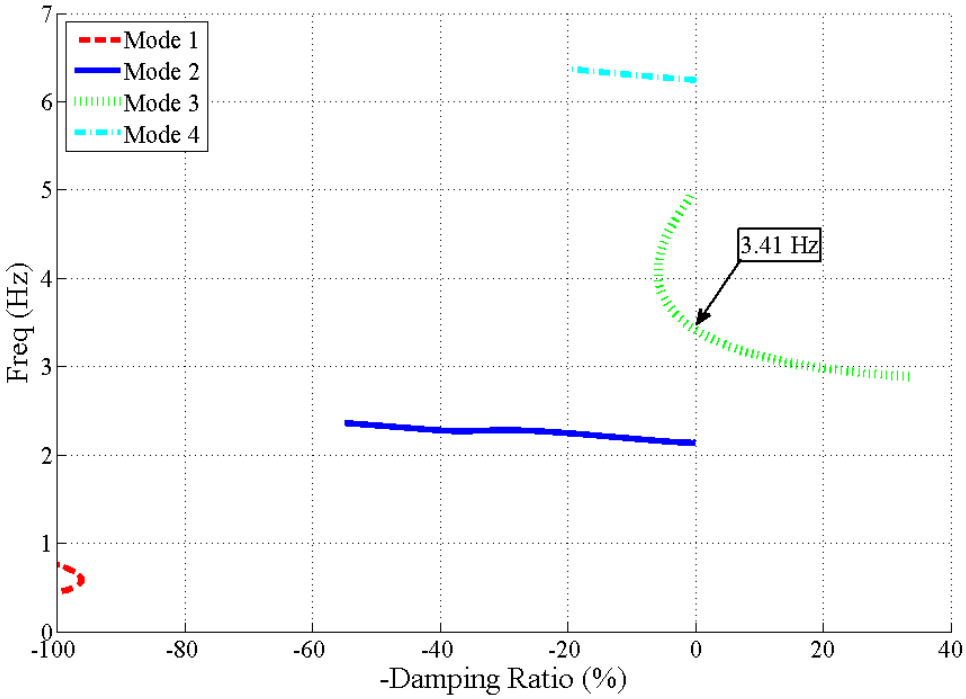

Figure 6.5 – Frequency vs. damping ratio root locus for HALE wing configuration

6.3. Model limitations

The beam representation for a wing structure can be valuable for early phases of aircraft design when sufficient data regarding the structure is not available. In the later stages of design, the complexities of aircraft components are difficult to model with a beam representation, and the analysis and certification of aircraft require a more detailed FE structural mesh. The logical extension of the

usage of beam structures is a coupling with compatible shell elements to allow for accurate modeling of the outer skin of a semi-moncoque structure. The use of shell elements to model the panels and beam elements to model the wing spars and booms allows for much more accuracy and is a common industrial practice [5]. However, the upgraded FE structural model does not give any benefit to the mass model of the aircraft since a significant portion of aircraft mass is non-structural such as payload and fuel. The upgraded structural model is usually condensed into a beam representation where only a select set of "master" DOF are considered [65]. The mass is often idealized as a beam, thus the original model proposed in this thesis is uniquely justified.

Accurate modeling of flutter phenomenon requires the most precise aerodynamic models with an inclusion of unsteady three-dimensional effects. The strip loading method is commonly used for airworthiness certification [5], but a panel method is a more accurate three-dimensional unsteady model. The strip loading model also cannot accurately represent transonic effects where flutter often occurs, therefore, a coupled CFD-structural FE model with fluid structural interaction must be used in highly nonlinear cases.

Chapter 7

Conclusion

7.1. Thesis Summary

The formulation of classical structural finite element methods with the inclusion of aerodynamic stiffness and damping effects has been covered. The free vibration modes of eccentric structures fundamentally determined the aeroelastic behavior, and a quintic interpolation of the assumed displacement shape accurately predicted the characteristic behavior with fewer elements. Static aerodynamics was used as the basis for loading applied to eccentric structures, and for consideration of time independent behavior of aeroelastic systems. The unsteady strip loading formulation was then used as a direct extension of static aerodynamics for a linear dynamic analysis in the frequency domain.

The frequency domain formulation of the characteristic aeroelastic equation led to a flutter boundary prediction with a frequency matching scheme and a modal

interaction illustration in the form of the $V\omega - Vg$ plots. The cubic interpolation element accurately predicted low order effects when higher characteristic frequencies were outside the range of interest as in binary flutter. However, the quintic interpolation better predicted higher order characteristic effects when multimodal interactions were important for low DOF flutter prediction, such as the HALE aircraft wing. The quintic interpolation aeroelastic element predicted essentially exact low and high modal solutions with a single element as compared to analytical solutions and finite element solutions with many elements. Thus, the quintic interpolation aeroelastic element seems to be a more powerful tool than the classical cubic interpolation element.

7.2. Further Research

Aeroelasticity is a growing field of importance as new and exotic methods of air and space transportation are explored. The computational formulation of an aeroelastic problem requires a background in every constituent field, and further research in applied mathematics, computational science, and aerodynamic loading is necessary for more advanced analysis. CFD based aeroelastic analysis seems to be the trend of current and potential research, but there are also many approximating techniques worth investigating. For example, the dynamic element method [28, 66] is a structural response approximation technique that expands the static interpolation function to include the frequency effects directly. The doublet-lattice method is an aerodynamic loading approximation technique common in industrial

practice that models the loading of discrete panels with bounded vortices producing accurate three-dimensional predictions. Similar approximate analysis techniques tend to achieve a much quicker solution, but usually at the cost of accuracy, so any further exploration of such techniques should be integrated into a compatible computation method.

References

[1] B. Long, "Latin Maxims IV," *Give me 5 minutes and I will give you the world*. 26-May-2005.

[2] A. Collar, "The first fifty years of aeroelasticity," *Aerospace*, vol. 5, no. 2, pp. 12–20, 1978.

[3] D. H. Hodges and G. A. Pierce, *Introduction to structural dynamics and aeroelasticity*. Cambridge University Press, 2002.

[4] E. H. Dowell, R. Clark, D. Cox, H. C. Curtiss, J. W. Edwards, K. C. Hall, D. A. Peters, R. H. Scanlan, E. Simiu, F. Sisto, and T. W. Strganac, *A modern course in aeroelasticity*. Springer, 2004.

[5] J. R. Wright and J. E. Cooper, *Introduction to aircraft aeroelasticity and loads*. John Wiley and Sons, 2007.

[6] R. L. Bisplinghoff, H. Ashley, and R. Halfman, *Aeroelasticity*. Cambridge, Mass., Addison-Wesley Pub. Co., 1955.

[7] I. E. Garrick and W. H. Reed, "Historical development of aircraft flutter," *Journal of Aircraft*, vol. 18, pp. 897–912, Nov. 1981.

[8] R. L. Bisplinghoff and H. Ashley, *Principles of Aeroelasticity*. Dover, 1975.

[9] K. K. Gupta and J. L. Meek, *Finite element multidisciplinary analysis*. AIAA, 2003.

[10] T. A. Weisshaar, "Static and Dynamic Aeroelasticity," *Encyclopedia of Aerospace Engineering*, p. 14, 2010.

[11] T. A. Weisshaar, "Introduction," Purdue University, 2010.

[12] K. Y. Billah and R. H. Scanlan, "Resonance, Tacoma Narrows bridge failure, and undergraduate physics textbooks," *Am, J. Phys*, vol. 59, p. 2, 1991.

[13] E. H. Dowell, "Panel flutter - A review of the aeroelastic stability of plates and shells," *AIAA Journal*, vol. 8, no. 3, pp. 385–399, Mar. 1970.

[14] M. D. Olson, "Finite Elements Applied to Panel Flutter," *AIAA Journal*, vol. 5, no. 12, pp. 2267–2270, Dec. 1967.

[15] N. Taylor, G. Vio, A. Rampurawala, C. Allen, D. Jones, K. Badcock, J. Cooper, A. Gaitonde, M. Henshaw, D. Jones, and M. Woodgate, "Aeroelastic simulation

through linear and non-linear methods: a summary of flutter prediction in the PUMA DARP," *Aeronautical Journal*, vol. 110, no. 1107, pp. 333–343, 2006.

[16] C. Mei, "A Finite-Element Approach for Nonlinear Panel Flutter," *AIAA Journal*, vol. 15, pp. 1107–1110, Aug. 1977.

[17] E. H. Dowell, "Nonlinear Oscillations of a Fluttering Plate," *AIAA Journal*, vol. 5, no. 10, pp. 1856–1862, Oct. 1967.

[18] M. J. Patil and D. H. Hodges, "On the importance of aerodynamic and structural geometrical nonlinearities in aeroelastic behavior of high-aspect-ratio wings," *Journal of Fluids and Structures*, vol. 19, no. 7, pp. 905–915, Aug. 2004.

[19] A. Namini, P. Albrecht, and H. Bosch, "Finite Element-Based Flutter Analysis of Cable-Suspended Bridges," *Journal of Structural Engineering*, vol. 118, no. 6, p. 1509, Jun. 1992.

[20] Y.-C. Fung, *An introduction to the theory of aeroelasticity*, (original 1955). Dover, 2008.

[21] C. A. Felippa, "A historical outline of matrix structural analysis: a play in three acts," *Computers & Structures*, vol. 79, no. 14, pp. 1313–1324, 2001.

[22] R. A. Frazer, W. J. Duncan, and A. R. Collar, *Elementary matrices and some applications to dynamics and differential equations*. Cambridge [Eng.] The University press, 1938.

[23] W. Duncan and A. Collar, "Matrices applied to the motions of damped systems," *Philosophical Magazine Series 7*, vol. 19, no. 125, pp. 197–219, 1935.

[24] C. F. Garland, "The normal modes of vibrations of beams having noncollinear elastic and mass axes," *J. appl. Mech*, vol. 7, p. A 97 – A 105, 1940.

[25] C. Mei, "Coupled vibrations of thin-walled beams of open section using the finite element method," *International Journal of Mechanical Sciences*, vol. 12, no. 10, pp. 883–891, Oct. 1970.

[26] E. Dokumaci, "An exact solution for coupled bending and torsion vibrations of uniform beams having single cross-sectional symmetry," *Journal of Sound and Vibration*, vol. 119, no. 3, pp. 443–449, Dec. 1987.

[27] R. E. D. Bishop, S. M. Cannon, and S. Miao, "On coupled bending and torsional vibration of uniform beams," *Journal of Sound and Vibration*, vol. 131, no. 3, pp. 457–464, Jun. 1989.

[28] J. R. Banerjee, "Coupled bending–torsional dynamic stiffness matrix for beam elements," *International Journal for Numerical Methods in Engineering*, vol. 28, no. 6, pp. 1283–1298, Jun. 1989.

[29] I. Kroo, "Linearization," *Aerodynamic Modeling for Simulation and Control*, Spring-2002. [Online]. Available: http://adg.stanford.edu/aa208/dynamics/linearization.html. [Accessed: 20-Feb-2012].

[30] T. Theodorsen, "General theory of aerodynamic instability and the mechanism of flutter," Unites States National Advisory Committee for Aeronautics, 496, Jan. 1935.

[31] T. Theodorsen and I. E. Garrick, "Mechanism of flutter a theoretical and experimental investigation of the flutter problem," Unites States National Advisory Committee for Aeronautics, 685, Jan. 1941.

[32] F. W. Lanchester, "The Development of the Military Aeroplane," in *Scientific American: Supplement*, vol. LXXXI, Munn and Co., 1916, pp. 364–365.

[33] H. J. Hassig, "Approximate true damping solution of the flutter equation by determinant iteration," *Journal of Aircraft*, vol. 8, pp. 885–889, Nov. 1971.

[34] F. W. Diederich, "Divergence of swept wings," DTIC Document, 1948.

[35] G. Herrmann, S. Nemat-Nasser, and S. N. Prasad, "Bending-torsional flutter of a swept wing in a high-density, low-speed flow.," *AIAA Journal*, vol. 5, no. 2, pp. 316–321, Feb. 1967.

[36] I. Lottati, "Flutter and divergence aeroelastic characteristics for composite forward swept cantilevered wing," *Journal of Aircraft*, vol. 22, no. 11, pp. 1001–1007, 1985.

[37] L. Librescu and O. Song, "On the static aeroelastic tailoring of composite aircraft swept wings modelled as thin-walled beam structures," *Composites Engineering*, vol. 2, no. 5–7, pp. 497–512, 1992.

[38] M. N. Nahas, "The Finite Element Technique in the Determination of Wing Flutter," *Journal of King Abdulaziz University : Engineering Sciences*, vol. 3, pp. 61–70, 1991.

[39] M. Goland, "The flutter of a uniform cantilever wing," *Journal of Applied Mechanics*, vol. 12, no. 4, p. A197–A208, 1945.

[40] X. G. Hua and Z. Q. Chen, "Full-order and multimode flutter analysis using ANSYS," *Finite Elements in Analysis and Design*, vol. 44, no. 9–10, pp. 537–551, Jun. 2008.

[41] T. A. Weisshaar, "Panel flutter optimization—a refined finite element approach," *International Journal for Numerical Methods in Engineering*, vol. 10, no. 1, pp. 77–91, Jan. 1976.

[42] C. E. Gray, C. Mei, and C. P. Shore, "Finite element method for large-amplitude two-dimensional panel flutter at hypersonic speeds," *AIAA Journal*, vol. 29, no. 2, pp. 290–298, Feb. 1991.

[43] D. Y. Xue and C. Mei, "Finite element nonlinear panel flutter with arbitrary temperatures in supersonic flow," *AIAA Journal*, vol. 31, no. 1, pp. 154–162, Jan. 1993.

[44] G. Cheng and C. Mei, "Finite Element Modal Formulation for Hypersonic Panel Flutter Analysis with Thermal Effects," *AIAA Journal*, vol. 42, no. 4, pp. 687–695, Apr. 2004.

[45] C. Spyrakos, *Finite element modeling in engineering practice*, vol. 1. West Virginia University Press and Algor Pittsburgh, PA, 1995.

[46] M. Petyt, *Introduction to finite element vibration analysis*. Paperback ed., 1998.

[47] S. S. Rao and R. S. Gupta, "Finite Element Vibration Analysis of Rotating Timoshenko Beams," *Journal of Sound and Vibration*, vol. 242, no. 1, pp. 103–124, Apr. 2001.

[48] F. Abassian, D. J. Haswell, and N. C. Knowles, *Free vibration benchmarks Volume 1*, vol. 1, 3 vols. Glasgow : NAFEMS., 1987.

[49] P. R. Heyliger and J. N. Reddy, "A higher order beam finite element for bending and vibration problems," *Journal of Sound and Vibration*, vol. 126, no. 2, pp. 309–326, Oct. 1988.

[50] J. E. Akin, "Quintic beam closed form matrices." http://www.clear.rice.edu/mech517/, 23-Feb-2012.

[51] J. R. Banerjee, "Explicit Frequency Equation and Mode Shapes of a Cantilever Beam Coupled in Bending and Torsion," *Journal of Sound and Vibration*, vol. 224, no. 2, pp. 267–281, Jul. 1999.

[52] T. A. Weisshaar, "Models and Concepts," Purdue University, 2010.

[53] B. K. Donaldson, *Analysis of aircraft structures : an introduction*, 2nd ed. Cambridge University Press, 2008.

[54] T. R. Yechout and S. L. Morris, *Introduction to aircraft flight mechanics: performance, static stability, dynamic stability, and classical feedback control*. AIAA, 2003.

[55] T. A. Weisshaar, "Stability," Purdue University, 2010.

[56] "FAR-25: Certification Specifications for FAA." [Online]. Available: http://www.faa.gov/. [Accessed: 01-Mar-2012].

[57] T. A. Weisshaar, "Unsteady Aerodynamics," Purdue University, 2010.

[58] A. R. Collar and A. Simpson, *Matrices and engineering dynamics*. Chichester [West Sussex]: E. Horwood; New York: Halsted Press., 1987.

[59] R. M. V. Pidaparti and C. C. Chang, "Finite element supersonic flutter analysis of skewed and cracked composite panels," *Computers & Structures*, vol. 69, no. 2, pp. 265–270, Oct. 1998.

[60] C. Hwu and M. Yu, "A comprehensive finite element model for tapered composite wing structures," *CMES - Computer Modeling in Engineering and Sciences*, vol. 67, no. 2, pp. 151–173, 2010.

[61] "Eigenvalues and eigenvectors," *MATLAB Product Documentation*, 2012. [Online]. Available: http://www.mathworks.com/help/techdoc/ref/eig.html. [Accessed: 27-Mar-2012].

[62] "Modified Bessel function of second kind," *MATLAB Product Documentation*. [Online]. Available: http://www.mathworks.com/help/techdoc/ref/besselk.html. [Accessed: 30-Mar-2012].

[63] F. Tisseur and K. Meerbergen, "The Quadratic Eigenvalue Problem," *SIAM Review*, vol. 43, no. 2, pp. 235–286, Jun. 2001.

[64] M. J. Patil, D. H. Hodges, and C. E. S. Cesnik, "Nonlinear aeroelasticity and flight dynamics of high-altitude long-endurance aircraft," *Journal of Aircraft*, vol. 38, no. 1, pp. 88–94, 2001.

[65] B. Irons, "Structural eigenvalue problems- elimination of unwanted variables," *AIAA journal*, vol. 3, p. 961, 1965.

[66] J. R. Banerjee, H. Su, and C. Jayatunga, "A dynamic stiffness element for free vibration analysis of composite beams and its application to aircraft wings," *Computers & Structures*, vol. 86, no. 6, pp. 573–579, Mar. 2008.

Appendix A

Explicit quintic bending element stiffness and mass matrices

$$m_{eC^2} = \frac{\mu L_e}{13860}\begin{bmatrix} 2092 & 114L_e & 880 & -160L_e & 262 & -29L_e \\ 114L_e & 8{L_e}^2 & 88L_e & -12{L_e}^2 & 29L_e & -3{L_e}^2 \\ 880 & 88L_e & 5632 & 0 & 880 & -88L_e \\ -160L_e & -12{L_e}^2 & 0 & 128{L_e}^2 & 160L_e & -12{L_e}^2 \\ 262 & 29L_e & 880 & 160L_e & 2092 & -114L_e \\ -29L_e & -3{L_e}^2 & -88L_e & -12{L_e}^2 & -114L_e & 8{L_e}^2 \end{bmatrix}$$

$$k_{eC^2} = \frac{EI}{35{L_e}^3}\begin{bmatrix} 5092 & 1138L_e & -3584 & 1920L_e & -1508 & 242L_e \\ 1138L_e & 332{L_e}^2 & -896L_e & 320{L_e}^2 & -242L_e & 38{L_e}^2 \\ -3584 & -896L_e & 7168 & 0 & -3584 & 896L_e \\ 1920L_e & 320{L_e}^2 & 0 & 1280{L_e}^2 & -1920L_e & 320{L_e}^2 \\ -1508 & -242L_e & -3584 & -1920L_e & 5092 & -1138L_e \\ 242L_e & 38{L_e}^2 & 896L_e & 320{L_e}^2 & -1138L_e & 332{L_e}^2 \end{bmatrix}$$